

| | | | |
|-----------------------------------|-------------------------|-------------------------|---------------------------|
| numerical aperture (N_A) | peak wavelength (PW) | rise time | thermal resistance |
| operating wavelength | photon density | sigma (σ) | thermoelectric aperture |
| optical efficiency | power dissipation | spectral bandwidth | threshold current |
| optical energy confinement factor | quality factor | spectral linewidth | threshold current density |
| output power | quantum efficiency | spontaneous emission | time domain |
| peak amplitude (PA) | quantum well (QW) | stimulation emission | transmissivity |
| peak excursion (PE) | laser | surface emitting LED | vertical cavity surface |
| peak function (PF) | radiative recombination | temperature coefficient | emitting laser |
| | reliability factor | temperature factor | (VCSEL) |

3.1 INTRODUCTION

The primary optical source of a fiber optics transmission system is the semiconductor **light emitting diode (LED)**. The selection of this device as the primary optical source was based on its ability to provide optical power ranging from 0.05 mW to 2 mW over optical fibers several kilometers in length. Semiconductor optical sources are very reliable devices with long operating life projections. Another advantage of the devices is that for ordinary system applications they require no modulating circuitry because the optical power of the device can be altered in accordance with the input current variations.

In the early 1970s the basic device structure was composed of **gallium arsenide (GaAs)** and **aluminum gallium arsenide (AlGaAs)** materials that were capable of generating wavelengths of 800 nm to 900 nm.

These LED devices were limited to short transmission optical links because the optical fibers' large signal attenuation at high data rates. Continuous improvement in optical fiber manufacturing technology, especially in the 1700 nm to 1500 nm wavelengths, significantly improved the overall data transmission capability of LED devices. The continuous drive to satisfy an ever-increasing system performance demand generated the need for the development of improved LED devices such as indium gallium arsenide phosphorus (InGaAsP). These devices were capable of generating light power covering the 920 nm to 1650 nm spectrum.

Today, two basic types of semiconductor optical sources exist. The LEDs we have just briefly described, and **laser diodes**. Laser diodes are used for long distance, high data rate transmissions, while LED devices are used for shorter distance, lower data rate transmission. The progressive evolution of LED technology led to the development of two types of LED devices: edge emitting LEDs (ELEDs), and surface emitting LEDs (SLEDs).

Edge emitting LEDs are used for both single-mode and multi-mode operations with bit rates in excess of 400 Mb/s. Lasers made their appearance in the early 1960s. However, these optical sources had to wait for another ten years for full implementation in optical communications systems. This was essential if improvements in areas such as photon confinement, excessive device degradations, improved stability, and forward current biasing requirements were to be made.

In the early 1970s, AlGaAs **heterojunction lasers** emitting at wavelengths between 800 nm and 4000 nm were already operational. To be compatible with optical fibers operating at wavelengths between 1000 nm and 2000 nm, laser diodes composed of AlGaAsSb/GaSb and InGaAsP/InP alloy structures were fabricated. Other diode structures, employing such alloys as GaAlInN and MgZnSSe, are already in the advanced state of development and are capable of emitting at blue and green wavelengths.

The demand for high bandwidths and long optical link distances accelerated the development of sophisticated laser structures. The evolution of advanced optical fibers, erbium-doped fiber amplifiers (EDFAs), optical add/drop multiplexers (OADM), Mach-Zehner modulators, and dispersion-compensation modules in the middle of 1990s, in conjunction with advanced laser diode designs made possible the development of **dense wavelength division multiplexing (DWDM)** optical systems. Laser diodes that required relatively low forward current to achieve lasing, and that exhibited characteristics such as high **optical efficiency**, very narrow **spectral linewidth**, higher optical power, and operating wavelengths between 630 nm and 1550 nm, and **operating wavelengths** were absolutely essential for the direct modulation capability were absolutely essential for the development of DWDM long distance optical links.

Since the 1990s, laser diode technology has dramatically improved device performance characteristics through the introduction of **vertical cavity surface emitting lasers (VCSEL)** and **quantum well (QW) lasers**. Such diodes exhibit a superior optical efficiency (conversion from electrical to optical power), tunable capabilities for a wide wavelength area, extremely high modulating rates (GHz), and very narrow line widths down to (KHz) range—all necessary parameters for implementation in DWDM optical systems.

Surface emitting LEDs are better suited to multi-mode, medium range optical fiber transmission. The fundamental theory for the design and construction of LED and laser optical sources is based on electron hole recombination within a semiconductor material. This electron hole recombination results in a generation of photons that have frequencies that are determined by the physical parameters of the semiconductor material. The two phenomena derived from the interaction between matter and light are **emission** and **absorption**. Emission can also be divided into two basic

DOMS Page No. 1 / 1

Date _____

Q. A photon diode has a bandgap energy of $E_g = 0.867 \text{ eV}$. If it is irradiated with a photon of $E = 1.42 \times 10^{-34} \text{ J}$, determine if it will detect radiation.

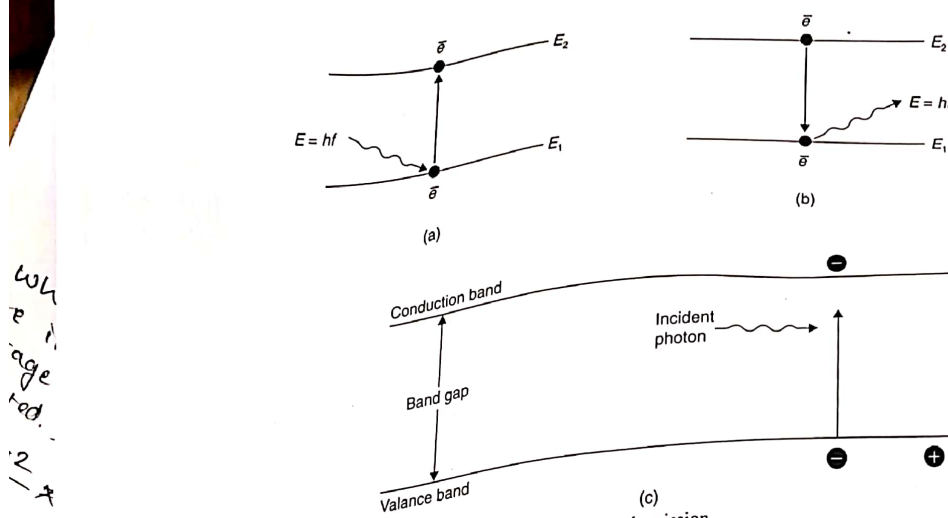


Figure 3-1. (a) Absorption, (b) spontaneous emission, and (c) stimulated emission.

categories: **stimulation emissions and spontaneous emissions**. Both stimulation emission and spontaneous emission can be better explained with the assistance of the following oversimplified atomic-model (Figure 3-1).

An electron of energy E_1 can be elevated to level E_2 by absorbing a photon of energy $E = hf$. An electron that is already at energy level E_2 can decay to energy level E_1 by releasing a photon (spontaneous emission). The third phenomenon is observed when an electron already at energy level E_2 absorbs a photon and decays to energy level E_1 . Through this process, two photons that have the exact same phase direction and energy levels are simultaneously released. If continuous radiation is maintained, the generation released. If continuous radiation is maintained, the generation of photons will also be continued (stimulation emission).

LED operation is based on spontaneous emission, while the laser operation is based on stimulated emission. In general, for both devices, the principle of operation is based on the interaction of light and matter within a semiconductor material.

3.2 LIGHT EMITTING DIODES (LEDS)

Perhaps the best representative of the optical source device family is that of the light emitting diode (LED). LEDs are classified as electro-luminescent devices that are composed of semiconductor materials that are capable of generating light when they are forward biased by a current source. Basic semiconductor materials that compose LED structures are GaAsP, GaAlAs, GaAs, and GaP. Gallium arsenide phosphide (GaAsP) LEDs generate light between 640 nm and

700 nm, with a peak optical power at 660 nm. Gallium aluminum arsenide (GaAlAs) LEDs produce light between 650 nm and 700 nm, with a peak optical power at 670 nm. Gallium phosphate (GaP) LEDs generate light between 520 nm and 570 nm, with a peak optical power at 550 nm. Indium gallium arsenide phosphorus devices are recent developments that present advantages over GaAsP semiconductor devices. These devices can generate optical wavelengths between 930 nm and 1650 nm. The selection of semiconductor materials and their proportional contribution to optical device fabrication is indicative of the wavelengths required. The optical energy obtained from semiconductor material combination is measured in electron volts (eV), as follows:

$$\begin{array}{ll} \text{Ge} = 0.7 \text{ eV} & \text{GaP} = 2.2 \text{ eV} \\ \text{Si} = 1.1 \text{ eV} & \text{GaAs} = 1.4 \text{ eV} \\ \text{CdS} = 2.4 \text{ eV} & \text{GaAlP} = 0.8 - 2.0 \text{ eV} \end{array}$$

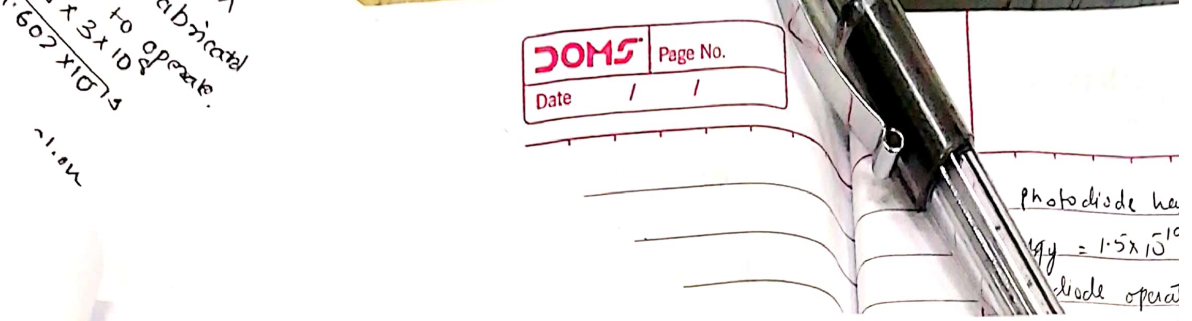
The center wavelength (λ_c) of an LED device is determined by the **band gap** energy (E_g) in eV at the active layer, given by Equation (3-1).

$$\lambda_c = \frac{hc}{E_g} \quad (3-1)$$

where h is Planck's constant ($6.63 \times 10^{-34} \text{ J/s}$), c is the velocity of light in vacuum ($3 \times 10^8 \text{ m/s}$), and E_g is the band gap (eV).

Edge Emitting LEDs

Edge emitting LEDs were first introduced in the mid-1970s. Their basic structure closely resembles the laser diode, with one fundamental difference. For laser diodes, positive



feedback is promoted in order to enhance stimulated emission, while with edge emitting LEDs, the feedback mechanism is suppressed for the exact opposite reason, to prevent the device from going to a saturated emission mode of operation. The **active layer** (of n -AlGaAs) thickness of $0.05\ \mu\text{m}$ is confined by two layers of p and n semiconductor materials, such as p -AlGaAs and n -AlGaAs with a thickness of $0.115\ \mu\text{m}$. External to these two optical guiding layers are another two layers of p^+ -GaAs and n^+ -GaAs with a corresponding thickness of $3.5\ \mu\text{m}$. The optical guide layers confine the generated light into the active layer. This represents an advantage when coupling the source to the optical fiber. The basic device structure is shown in Figure 3-2.

An external DC source, connected across the device, will provide the necessary **forward biasing voltage**. The ejected electrons from the n -AlGaAs and holes from the p -AlGaAs layers will recombine at the thin n -AlGaAs layer. During the recombination process, a certain number of photons will escape through the edge of the active layer. By reducing the active layer, self-absorption is kept at a minimum, thus eliminating the possibility of stimulation emission. A typical voltage/current characteristic curve of an edge emitting LED (E-LED) is shown in Figure 3-3.

Figure 3-3 shows the current increasing exponentially beyond the threshold biasing voltage, which is characteristic of the device. The current (I) generated by the **forward biasing voltage** of the E-LED device is used to determine the optical power generated by that device (see Figure 3-4).

LED Characteristics

One of the most important characteristics of an LED source is that of power efficiency. Power efficiency is subdivided into two categories: **internal power effi-**

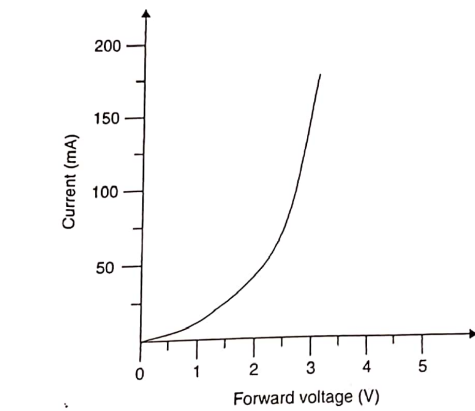


Figure 3-3. A typical voltage/current characteristic curve.

ciency, also called quantum efficiency (η_g), and **external power efficiency** (η_c).

Internal power efficiency is defined as the ratio of photons generated to the number of electrons induced into the active layer of the device (see Equation (3-2)).

$$\eta_g = \frac{N_{ph}}{N_{e^-}} \quad (3-2)$$

where η_g is the **quantum efficiency (%)**, N_{ph} is the number of photons, and N_{e^-} is the number of electrons. External power efficiency (η_c) is defined as the ratio of the optical power coupled into the fiber to the electrical power applied by the optical device (see Equation (3-3)).

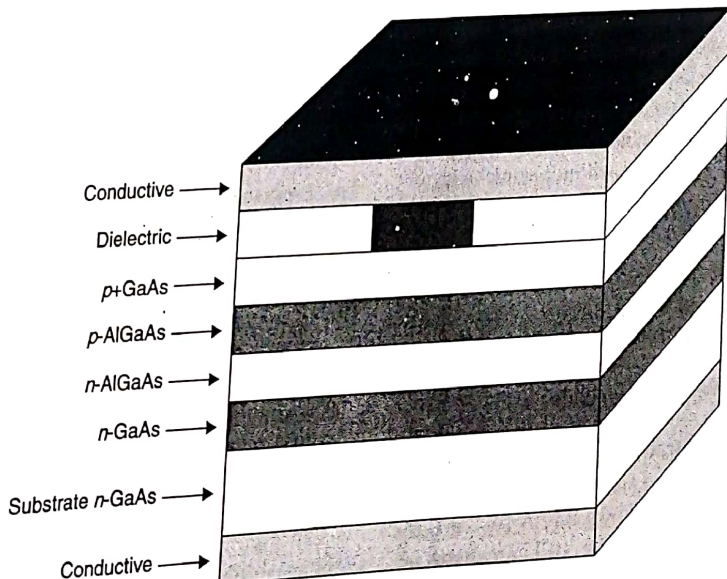


Figure 3-2. Edge emitting LED device structure.

Date: 12/20/2023
Page No.: 180

Ques. 1. A 1.5V 0.5A LED is coupled to a fiber with a numerical aperture of 2.5. Calculate the incident power required to operate a collector average of 3x10¹⁰ photons.

$P_o = 0.696 \text{ mW}$

$\frac{J_P}{P_o} = \frac{2.5 \times 10^{10}}{0.696}$

$P_o = 3 \times 10^{10} \text{ photons}$

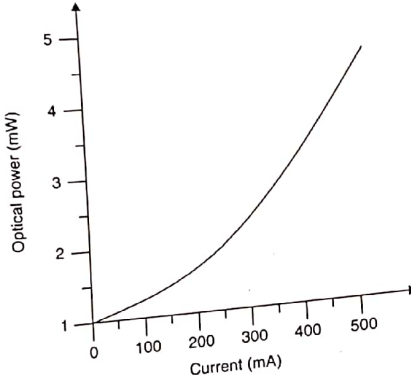


Figure 3-4. Current/optical power output characteristic curve.

$$\eta_c \% = \frac{P_F}{P_{in}} \times 100 \quad (3-3)$$

where η_c is the external power efficiency, P_F is the optical fiber power, and P_{in} is the input power.

Optical fiber power (P_F) is only a fraction of the power generated internally by the optical device. This optical power loss is relevant to the device-optical fiber coupling efficiency expressed by Equation (3-4).

$$\eta_c = (NA)^2 \quad (3-4)$$

where NA is the **numerical aperture** of the optical fiber.

Example 3-1
A light source generating an optical power output equal to 1 μW is coupled into an optical fiber with a cross sectional area larger than that of the active area of the light source.

Determine the power coupled into the fiber with a fiber θ° equal to 15° .

Solution

$$\theta = 15^\circ$$

Therefore, $\sin 15^\circ = NA$.

$$\sin(15^\circ) \approx 0.26 = NA$$

Coupling efficiency: $\eta_c = (NA)^2 = (0.26)^2 = 0.0676$

Power coupled into the fiber: $\eta_c = \frac{P_F}{P_{in}}$

$$\text{or } P_F = \eta_c \times P_{in} = 0.0676 \times 1 \mu\text{W} = 67.6 \text{ nW.}$$

Therefore, $P_F = 67.6 \text{ nW.}$

It is evident from the above example that only a small fraction of the optical power generated in the active region of the optic device will be coupled into the optical fiber.

Example 3-2
Calculate the optical power coupled into the fiber, generated by an optical source with a bias current of 20 mA and forward voltage of 1.5 V. The source internal efficiency is 2% and the fiber $\theta^\circ = 20^\circ$.

Solution

Power input to the optical device:

$$P_{in} = I_F \times V_F = 1.5 \text{ V} \times 20 \text{ mA} = 30 \text{ mW}$$

$$\therefore P_{in} = 30 \text{ mW}$$

The power output of the optical source is given by: $\eta_{in} = \frac{P_o}{P_{in}}$

$$\text{or } P_o = \eta_{in} \times P_{in} = 0.02 \times 30 \text{ mW} = 0.6 \text{ mW.}$$

Therefore, $P_o = 0.6 \text{ mW}$. This power output (P_o) of the optical source becomes the power input to the optical fiber.

$$P_{in} = 0.6 \text{ mW}$$

From $\eta_c = \frac{P_F}{P_{in}}$, solve for P_F .

$$P_F = \eta_c \times P_{in}$$

and $\eta_c = (NA)^2$ where $NA = (\sin \theta)^2$.

$$\text{Therefore, } \eta_c = (\sin 20^\circ)^2 = 0.116.$$

$$\text{Substituting into } P_F, P_F = \eta_c \times P_{in} = 0.116 \times 0.6 \text{ mW} = 0.0696 \text{ mW.}$$

Therefore, the optical power coupled into the optical fiber is:

$$P_F \approx 70 \mu\text{W.}$$

A more detailed relationship establishing the maximum power coupled into the optical fiber is given by Equation (3-5).

$$P_{Fmax} = I_o A_{min} \pi (NA)^2 \quad (3-5)$$

where P_{Fmax} is the maximum power coupled into the fiber, A_{min} is the minimum cross section area (selected between the active region of the optical source, or the cross section area of the fiber), NA is the numerical aperture of the fiber, and I_o is the ratio of the source optical power output and active area.

LED Spectral Bandwidth at the Half Power Point ($\Delta\lambda$)

The **LED spectral bandwidth (LED bandwidth)** determined at the **half power point (50%)** of the spectral density in reference to wavelength is illustrated in Figure 3-5.

LED optical devices exhibit a spectral bandwidth of between 20 nm and 200 nm at the half power point. This spectral bandwidth is translated to the pulse broadening as it travels through the optical fiber per kilometer of fiber length. LEDs emitting at peak wavelength of 800 nm exhibit a pulse broadening of 5 ns/km. This disadvantage of the LED device can be controlled by shifting the peak wavelength from

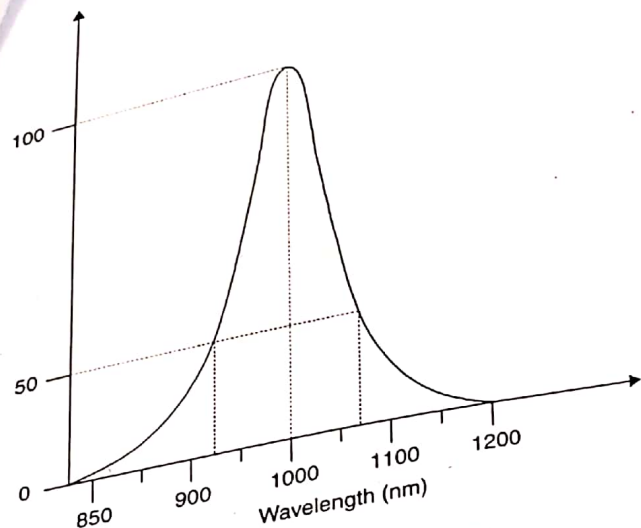


Figure 3-5. An LED spectral bandwidth curve.
800 nm to 1300 nm. At this wavelength, a smaller dispersion is encountered.

LED Bandwidth

Light emitting diodes are intensity modulated devices. That is, the input current can directly affect the output intensity of the device. In digital transmission, the LED device is turned ON and OFF in accordance with the input binary data. Ideally, turning ON and OFF the device must occur simultaneously with the input binary data. In reality there is a time delay between the bias current changes and turning ON and OFF the LED. This delay is caused by the **rise time** (t_r) and **fall time** (t_f) of the LED source (Figure 3-6).

Rise time (t_r) is measured between 10% and 90% of the power output. That is the time it takes the **output power** to increase from 10% to 90%. Fall time (t_f) is the time it takes the output to decrease from 90% to 10%. Rise time and fall time are the two most significant factors contributing to LED bandwidth limitations, which in turn establish the maximum data bit rate the device is capable of handling. This total time delay is the result of factors such as carrier recombination, time and space charge capacitance inherent to the LED device physical dimensions, and semiconductor properties. The equation that establishes total optical bandwidth at the half power point is given by Equation (3-6).

$$B_w = \frac{1}{2\pi r} \quad (3-6)$$

where B_w is the bandwidth and r is the **carrier lifetime** or **carrier recombination**.

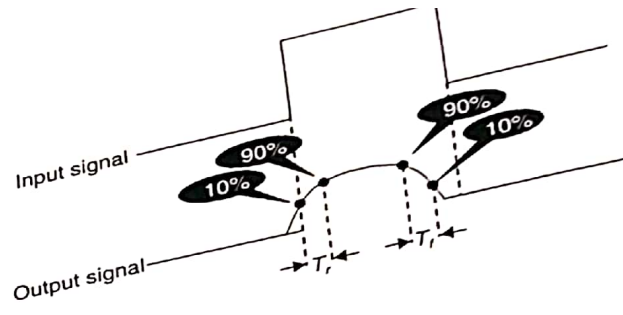


Figure 3-6. Time delay.

A more practical formula that establishes optical bandwidth is given by Equation (3-7).

$$B_w = \frac{0.35}{t_r} \quad (3-7)$$

where t_r is the rise time.

Example 3-3

Determine the bandwidth of an LED source with a rise time equal to 10 ns.

Solution

$$B_w = \frac{0.35}{t_r} = \frac{0.35}{10 \times 10^{-9} \text{ s}} = 35 \times 10^6 \text{ Hz}$$

$$B_w = 35 \text{ MHz}$$

Therefore, 35 MHz is the maximum operating bandwidth of this LED source.

The **modulation bandwidth** of an LED device can be increased by increasing the carrier concentration in the active region, with a simultaneous decrease of the carrier lifetime. This, of course, has a negative effect on the LED overall optical output power. Therefore, a compromise between modulation bandwidth and power output must be reached during the design process.

Surface Emitting LED

The design of a surface emitting LED (SLED) was based on a massive electron injection into a thin, optically transparent layer of *p*-material. This thin layer, confined between two other layers with larger band gaps, secures the confinement of the injected carriers, thus promoting a higher degree of recombination and a larger number of photon generations (see Figure 3-7).

In contrast to edge emitting LEDs, the optical radiation of the surface emitting LED takes place from the surface of the active layer. An examination of an SLED cross section reveals the following: The SiO_2 layer acts as an insulator between the GaAs *p*-layer and metallic conduct. The other two AlGaAs and GaAs *p*-materials are performing dual functions: light

Calculate MTBF:

$$MTBF = \frac{1}{R_f} = \frac{1}{5.46 \times 10^{-4}} = 18 \times 10^6$$

Therefore, MTBF = 8×10^6 hours.

Example 3-7
Compute the MTBF of an LED device operating at 60°C and
with electrical parameters as follows:

- Operating frequency: 50 MHz
- Peak drive current: 125 mA
- Forward voltage: 1.8 V

Solution
i) Compute R_f

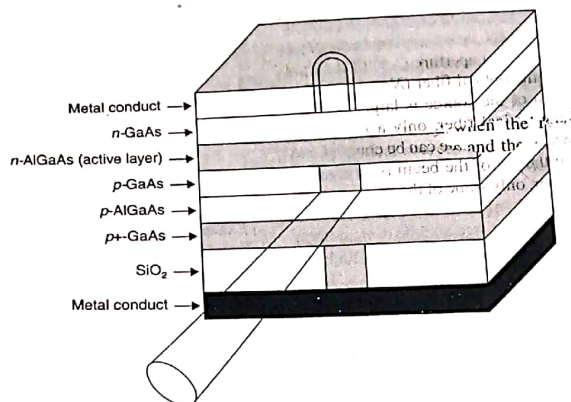


Figure 3-7. SLED cross section.

confinement and minimization of the recombination process close to the *p*-GaAs and *n*-AlGaAs junction.

The active region substrate of the SLED device is etched away in a well-type manner. This reduction of the active region dramatically reduces the recombination process, while the well-shaped area enhances the focus of the emitted light into the optical fiber. Another structure of an SLED semiconductor device is shown in Figure 3-8.

The SLED optical source shown in Figure 3-8 is designed to generate optical power in the 1.3 μm range. It uses an InP substrate because InP is transparent to this wavelength. The other four layers are grown epitaxially on this substrate, with varying doping levels and thicknesses in order to facilitate the device's design objectives (maximization of optical power and modulation speed). The first layer grown on the wafer substrate is a buffer composed of *n*-InP substance with an average thickness of 3 μm and a **doping density** of $2 \times 10^{18}/\text{cm}^3$.

The second layer is the much thinner active layer of *p*-InGaAsP substance, with an average thickness of 1 μm doped with Zn to an average density of $2 \times 10^{18}/\text{cm}^3$.

The third layer is the cladding layer, which is somewhat thicker than the first layer, with an average thickness of 2.5 μm and, similarly, doped with Zn to an average density of $2.75 \times 10^{18}/\text{cm}^3$. The fourth and final layer is composed of a very thin (0.25 nm) layer of *p*-ZnGaAsP substance, which is heavily *p*-doped and is intended to minimize conduct resistivity.

Coupling SLED Devices into Optical Fiber

One of the major problems inherent to optical fiber communication systems is that of the coupling of optical power, that is generated by the optical source, into the optical fiber. The

ratio of the optical power coupled into the fiber to the power generated by the optical source is called the **coupling efficiency** and is given by Equation (3-8).

$$\eta_c = \frac{P_f}{P_s} \quad (3-8)$$

where η_c is the coupling efficiency, P_f is the optical power coupled into the fiber, and P_s is the optical power generated by the source.

The inability to transfer all the generated optical power of the source into the fiber is caused by the different physical

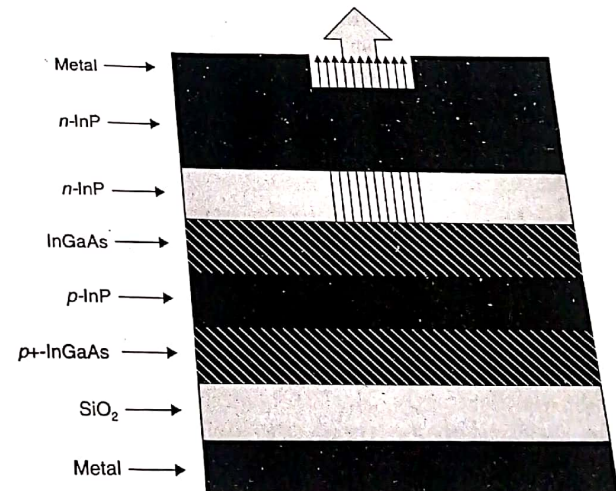


Figure 3-8. SLED device structure.

iii) Calculate MTBF

$$MTBF^f = \frac{1}{R_f} = \frac{1}{5.46 \times 10^{-8}} = 18 \times 10^6$$

Therefore, $MTBF^f = 18 \times 10^6$ hours.

Example 3-7
Compute the MTBF of an LED device operating at 80°C and with electrical parameters as follows:

- Operating frequency: 50 MHz with 50% duty cycle
- Peak drive current: 125 mA
- Forward voltage: 1.8 V

Solution

i) Compute (R_f).

$$R_f = B_F T_F E_F Q_F \frac{\text{failure}}{1 \times 10^6}$$

where $B_F = 6.5 \times 10^4$, $E_F = 0.75$ (from tables), and $Q_F = 0.2$ (from tables).

ii) Compute (T_F).

$$T_F = 8.01 \times 10^{12} e^{-\left(\frac{8111}{T_f + 273}\right)}$$

iii) Compute (T_J).

$$T_J = T_A + \theta_{JA} P_d$$

iv) Compute (P_d).

$$\begin{aligned} P_d &= I_F \times V_F \\ &= (0.5)(120 \text{ mA})(1.8 \text{ V}) \\ &= 0.108 \text{ W} \\ T_J &= 75 + \left(150 \frac{^\circ\text{C}}{\text{W}}\right)(0.108 \text{ W}) \\ &= 91.2^\circ\text{C} \end{aligned}$$

Therefore,

$$\begin{aligned} T_J &= 91.2^\circ\text{C} \\ T_F &= 8.01 \times 10^{12} e^{-\left(\frac{8111}{91.2 + 273}\right)} \\ &= 1704 \end{aligned}$$

$$\begin{aligned} R_f &= B_F T_F E_F Q_F \frac{\text{failure}}{1 \times 10^6 \text{ hr}} \\ &= (6.5 \times 10^4)(1704)(0.75)(0.2) \frac{\text{failure}}{1 \times 10^6 \text{ hr}} \\ &= 0.166 \times 10^{-6} \end{aligned}$$

Therefore, $R_f = 0.166 \times 10^{-6}$.

Finally, $MTBF^f = \frac{1}{R_f} = \frac{1}{0.166 \times 10^{-6}} = 6 \times 10^6$
Therefore, $MTBF^f = 6 \times 10^6$ hours.

3.3 LASER DIODES

Laser is an acronym for Light Amplification by Stimulated Emission of Radiation. Laser devices were first introduced in 1961, and their operations were based on stimulated emission instead of spontaneous radiation emission. Stimulated emission of radiation is the process whereby photons are used to generate other photons that have the exact phase and wavelength as the parent photons (Figure 3-14).

Fabry-Perot Lasers

Laser diodes are semiconductor devices capable of generating highly directional optical beams of particular wavelengths. Another important characteristic of laser diodes is that they can be modulated by very high rates, perhaps as high as 10 GHz.

These two very important characteristics make laser diodes ideal for applications in optical communications systems. However, laser diodes suffer from three inherited but very fundamental problems when employed as source devices in optical communications systems:

- a) laser diode temperature sensitivity
- b) back reflections
- c) susceptibility to optical interference

The **Fabry-Perot** laser structure is a simpler laser diode in comparison with LEDs capable of producing optical beams that have substantially wider spectral bandwidths. The only drawback of the Fabry-Perot structure is that it exhibits a higher degree of chromatic absorption, an unwanted component, that imposes limits on the overall performance of optical communication systems.

Emphasizing once more the basic difference between LED and Fabry-Perot diodes; LEDs generate optical power through spontaneous emission of radiation while Fabry-Perot structures generate optical power through stimulation emission of radiation.

Photon generation within a Fabry-Perot device starts with spontaneous emission. The initial photons trigger the generation of more electron-hole recombination, which in turn generates additional photons, and so on. Examining the stimulation emission of radiation reveals that a laser diode performs two basic functions: It initiates optical power generation of a specific wavelength and at the same time it amplifies this optical power to a level determined by the semiconductor materials used in the fabrication of the device and its physical characteristics. To achieve optical amplification, Fabry-Perot devices employ reflective mirrors on both sides of the photon traveling path (Figure 3-15).

CR SEX CNL
DNA-9619090584

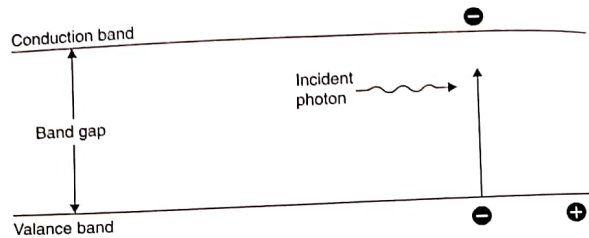


Figure 3-14. Stimulated emission of radiation.

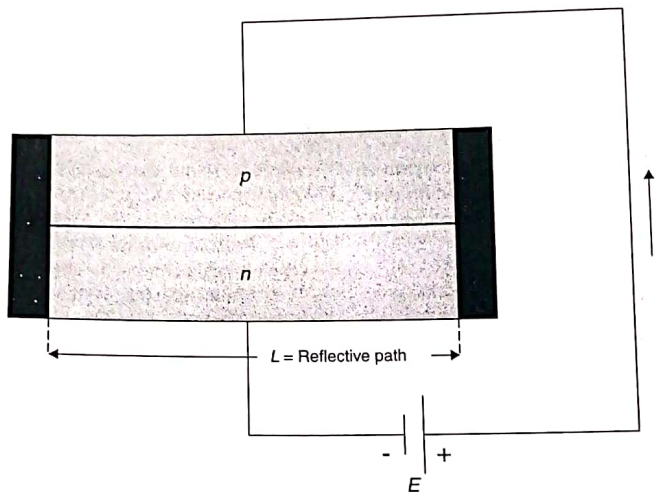


Figure 3-15. Simplified Fabry-Perot semiconductor structure.

These mirrors reflect the photons through the band gap, thus allowing for additional electron-hole recombination and larger photon generation. Not all the photons travelling between the reflective mirrors will contribute to optical amplification of the laser structure. These photons, which are in phase at a specific wavelength, will contribute to light amplification. Other photons, at different wavelengths, will contribute (to a lesser extent) to light amplification of other wavelengths. Again, the physical dimensions of the Fabry-Perot structure will determine the principal wavelength, achieving the highest optical gain. That is, if the mirror spacing is an integer number of half wavelength ($\lambda/2$), then the maximum optical amplification will occur in that wavelength while lesser optical amplification will be observed at the wavelength adjacent to the main. The optical spectrum of a Fabry-Perot resonator is illustrated in Figure 3-16.

The number of wavelengths that can be generated by a Fabry-Perot laser diode is given by Equation (3-17).

$$f_{\text{res}} = \frac{mc}{2ln} \quad (3-17)$$

OPTICAL SOURCES

where c is the velocity of light (3×10^8 m/s), m is the integer, l is the length between mirrors, and n is the **cavity refractive index**, and $\lambda = \frac{\lambda_o}{n}$

where n is the refractive index of the material. The spectral optical power density of Figure 3-16 shows that there is a separation between the different wavelengths around the center wavelength. This modal separation is a direct function of the distance between the two mirrors and is expressed by Equations (3-18) and (3-19).

$$\text{Spacing}_{\text{Modal}} = \frac{c}{2ln} \text{ (Hz) (frequency domain)} \quad (3-18)$$

where c is the velocity of light (3×10^8 m/s), l is the length between mirrors (**cavity length**), and n is the cavity reflective index, or

$$\text{Spacing}_{\text{Modal}} = \frac{\lambda^2}{2ln} \text{ (m) (time domain)} \quad (3-19)$$

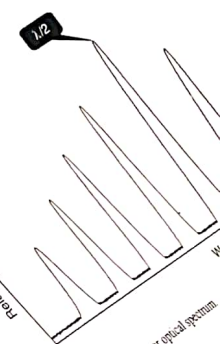


Figure 3-16. Fabry-Perot resonator optical spectrum where λ is the wavelength of the center wavelength and calculations must be done to define and discuss them in section 3-16.

TERVIS AND P
put (P_{r}). The
devices is def
by P

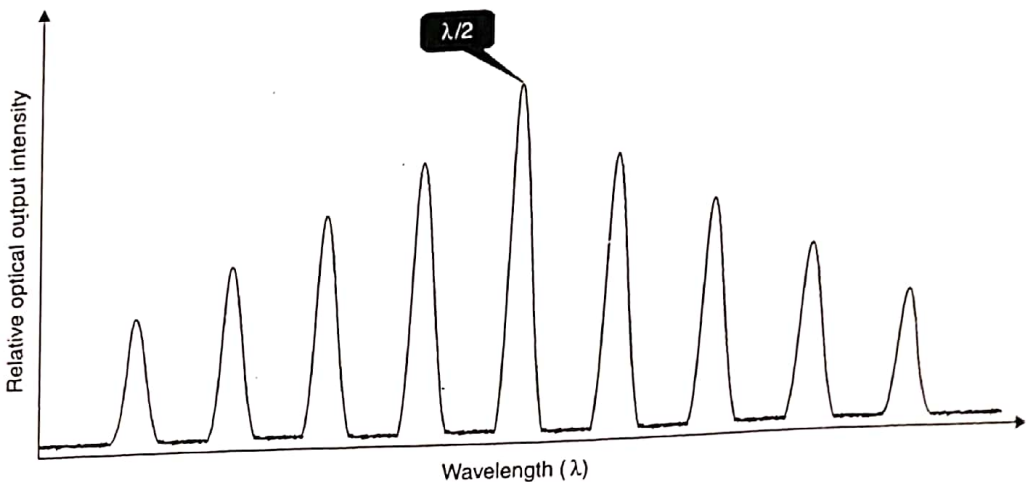


Figure 3-16. Fabry-Perot resonator optical spectrum.

where λ is the wavelength of the center mode. To evaluate the performance of a Fabry-Perot laser structure, certain measurements and calculations must be performed. Therefore, we will define and discuss them in some detail.

TERMS AND DEFINITIONS. *Total optical power output* (P_{TO}). The optical power output of a Fabry-Perot laser device is defined as the total sum of all the spectral components displayed by the optical spectral analyzer and set forth by **peak excursion** criteria (Equation (3-20)).

$$P_{TO} = \sum_i^N P_i \quad (3-20)$$

where N is the number of spectral components and P_i is the power of each spectral component.

Full Width at Half Maximum: For a continuous Gaussian power distribution (CGPD), **full width at half maximum (FWHM)** is defined as the optical power spectral density at half of the peak amplitude.

Mean wavelength (MW) defines the center of all the spectral components and is calculated by incorporating all the modal components in terms of their wavelengths and optical power. Mean wavelength is expressed by Equation (3-21).

$$\bar{\lambda}_{MW} = \sum_i^N P_i \left(\frac{\lambda_i}{P_o} \right) \quad (3-21)$$

where $\bar{\lambda}$ is the mean wavelength, P_i is the power of individual modes, P_o is the total optical output power, and λ_i is the modal wavelength. **Sigma (σ)** is defined as the Fabry-Perot laser root-mean-square of the spectral width, assuming Gaussian spectral distribution. It is calculated as follows in Equation (3-22).

$$\sigma = \sqrt{\frac{\sum_i^N P_i (\lambda_i - \bar{\lambda})^2}{P_o}} \quad (3-22)$$

where σ is the root-mean-square, P_o is the total optical output power, and λ_i is the wavelength of the individual modal component.

Peak amplitude (PA) defines the Fabry-Perot laser's center modal component amplitude.

Mode spacing is the average wavelength spacing between individual spectral modes.

Peak wavelength (PW) spacing in a Fabry-Perot laser diode is the wavelength with the highest amplitude within the total spectrum.

Peak function (PF): A single line can represent each component of the displayed spectrum. The display of this line indicates whether an adjustment is required for the peak excursion value (see peak excursion).

The **distribution trace (DT)** displays a more complete picture of the Fabry-Perot laser diode. This curve is Gaussian, and it represents a continuous approximation of the discrete spectrum that encompasses all the individual components, such as total optical output power, modal wavelengths, modal spacing, and mean wavelengths (Figure 3-17).

The **peak excursion (PE)** function of an optical spectrum analyzer allows for the adjustment of the base level of all the discrete spectral components. This is a critical adjustment because if it is not carefully set, it will result in either failure to detect useful spectral components near the noise level, or it will induce unwanted noise components in the useful spectrum.

Early in their development stage, laser devices exhibited a substantial increase in optical power output, confined to a very narrow beamwidth, in comparison with standard LED devices. Some of these early structures were based on heavily pumped ($2 \times 10^{18} \text{ e}/\text{cm}^3$), thin ($0.2 \mu\text{m}$) GaAs alloy forming the laser cavity and sandwiched between four **epitaxially grown** layers of AlGaAs, providing carrier and optical power confinement (see Figure 3-18).

For stimulation emission to occur, the number of electrons in the conducting band must exceed the number of electrons in the valence band. This increase can be accom-

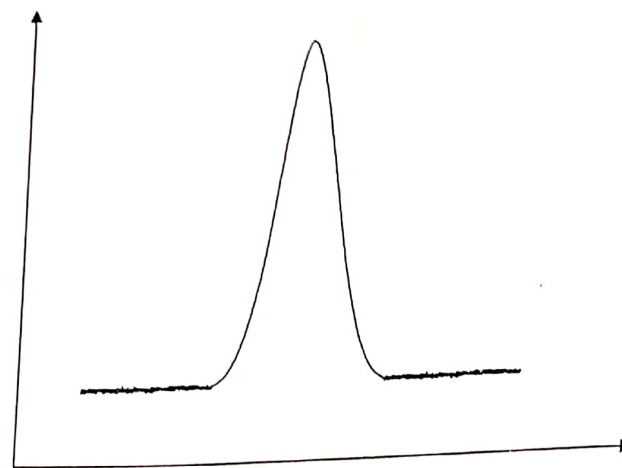


Figure 3–17. A distribution trace for a Fabry-Perot laser diode.

plished through the process of **pumping**. Pumping, or the elevation of electron from the valence band to the conducting band, is achieved by passing a sufficient amount of current through the active region of the laser device. Stimulated emission of radiation will start to take place at a minimum current level at the active region of the laser structure, called the *threshold current*. Below this threshold current, stimulated emission does not take place because radiation and absorption losses occurring inside the active region offset the additional photon generation below the threshold current. The relationship between threshold current and optical power output of a laser device is illustrated in Figure 3–19.

Figure 3–19 shows that at approximately 50 mA of injected current into the active region of the laser device, stimulated emission of radiation begins. Below 50 mA, the device operates under the spontaneous emission of radiation

mode. The early laser structures suffered from a lack of efficiency, that is, the electron-to-photon conversion ratio was low. In addition, they required very high currents, around 50 KA/cm^2 of active area, for stimulation emission to take place. These deficiencies of early laser diodes were addressed with the introduction of the double heterostructure laser device. A very thin low band gap, high refractive index AlGaAs active layer is confined between *n*-AlGaAs and *p*-AlGaAs layers with higher band gaps and lower refractive indexes (Figure 3–20).

In 1975, a threshold current of 0.5 KA/cm^2 was achieved in a laser device with an active layer of $0.1 \mu\text{m}$ thickness. This device was capable of generating optical power in the range of 800 nm to 900 nm. The optical wavelength generated by the laser device is related to the alloy composing the structure, and is expressed by Equation (3–23).

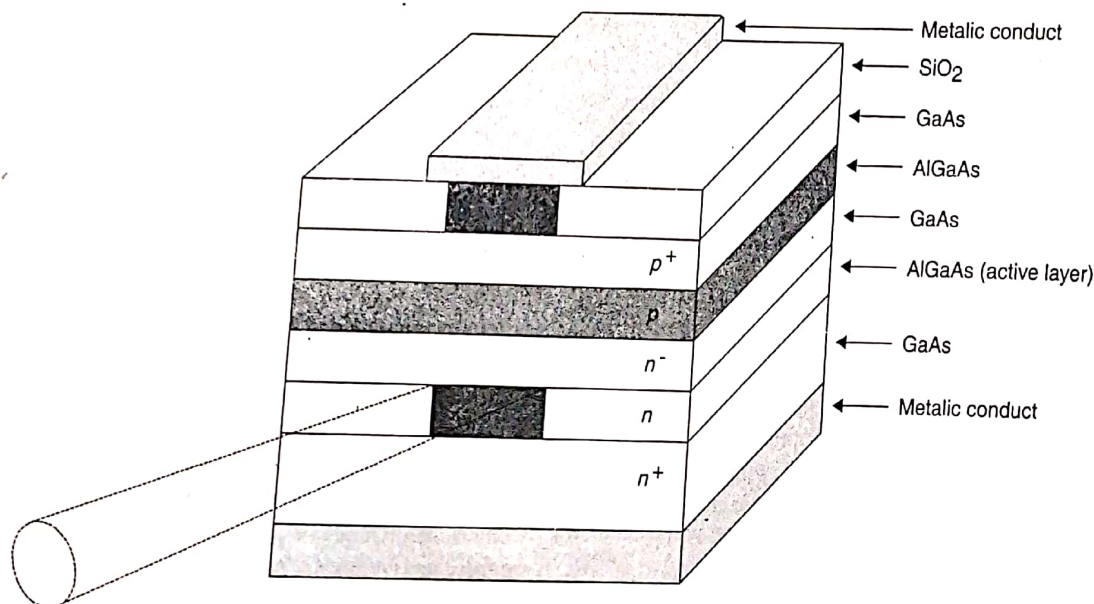


Figure 3–18. Fabry-Perot AlGaAs/GaAs laser diode.

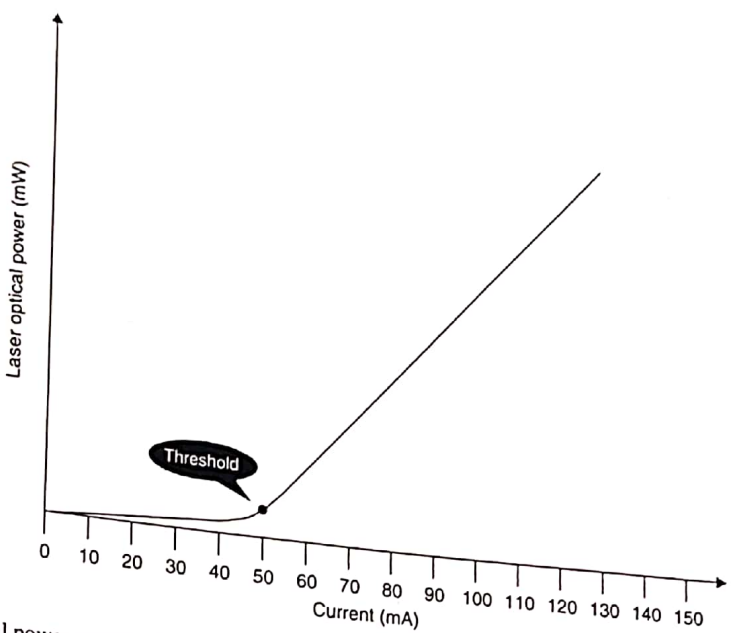


Figure 3-19. Laser optical power output v. biasing current

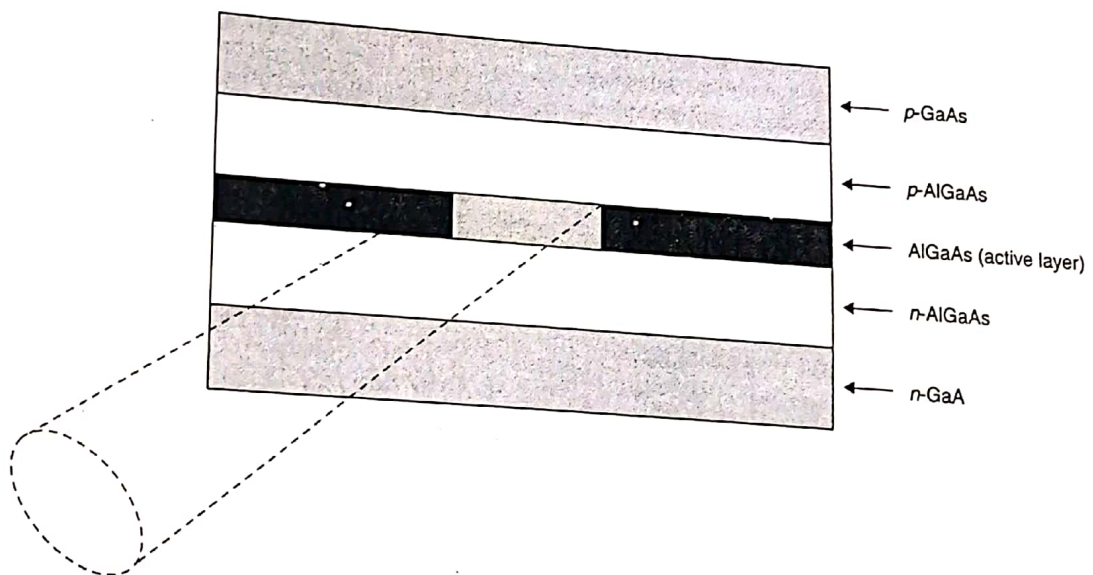


Figure 3-20. Fabry-Perot thin layer (AlGaAs/GaAs) laser diode.

$$\lambda = \frac{hc}{E_g} \quad (3-23)$$

where λ is the wavelength (nm), h is the Planck's constant (6.63×10^{-34} J/s), c is the velocity of light (3×10^8 m/s), and E_g is the band gap energy of the active region (eV).

For the InGaAsP alloy, $E_g = 0.74$ to 1.13 eV.

For the AlGaAs alloy, $E_g = 1.42$ to 1.61 eV.

For operating wavelengths in the spectral region between 1300 nm and 1500 nm, substances such as InGaAsP were introduced for the fabrication of laser semiconductor

structures that required a threshold current of 0.7 KA/cm 2 to 1.8 KA/cm 2 . The schematic diagram of such a device is shown in Figure 3-21.

If a forward biasing voltage between 1.5 V and 2.0 V is applied across the laser diode, a carrier concentration will gradually be built up into the active region. This carrier concentration is denser at the center of the active region than in the lateral regions. The high carrier density at the center of the active region far exceeds the transparency concentration, which results in an overall optical gain. The lesser lateral carrier concentration is far below the transparency level, thus

In optical fiber communications systems, direct optical modulation of the optical source is an established practice. At very high rates of modulation, the behavior of a single mode optical source begins to change, resulting in an output spectrum that shows more than one spectral line. In order to maintain a single mode spectral output, a modified version of the single-step index laser device is fabricated, this is a distributed-feedback laser (DFB).

Distributed Feedback Laser Structures

Careful examination of the spectral display of a laser diode reveals that it is composed of several (amplitude) modal component and several that have progressively lower amplitude.

This is a definite disadvantage of communications systems because it significantly increases chromatic dispersion of the output spectrum that is required for such applications will require a component of set amplitude.

In DFBs (see), the center have amplitude is to generate a data rates of m corrugated refracti

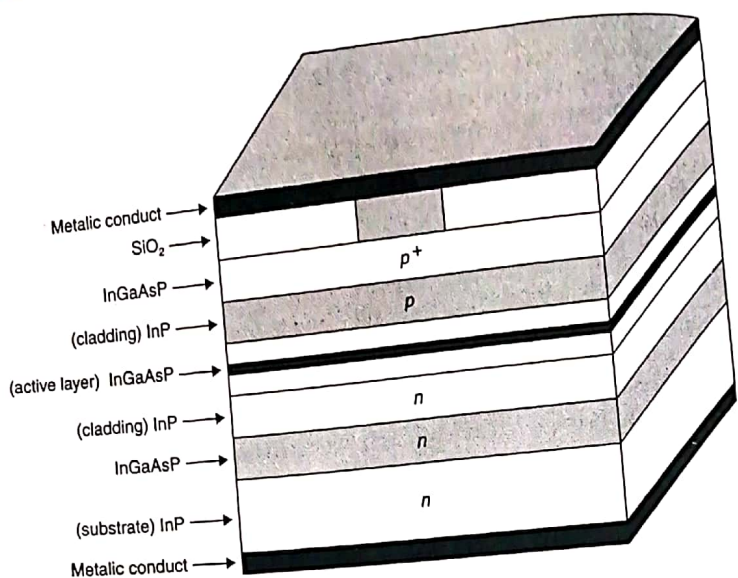


Figure 3-21. InGaAsP laser diode structure.

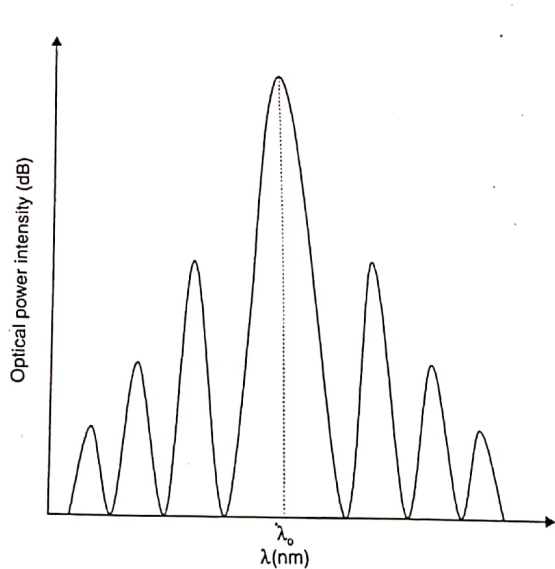


Figure 3-22. Spectral density.

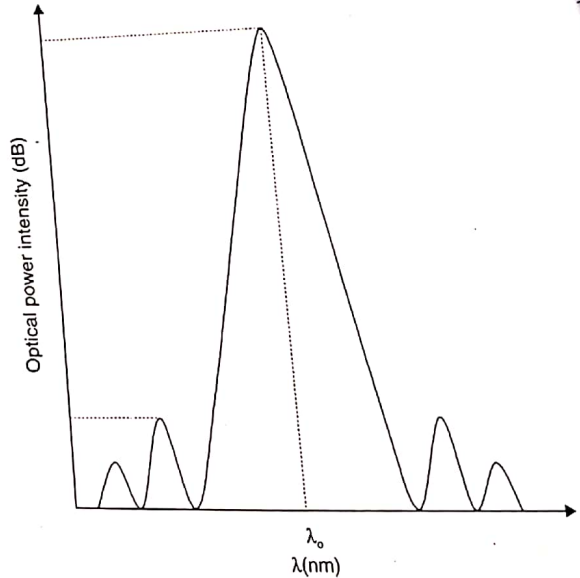


Figure 3-23. Laser diode spectral line.

an overall optical power loss is encountered in the lateral regions of the active layer. The double heterostructure laser is a gain guided multi-mode device. The spectral density of such a device is shown in Figure 3-22.

The multi-mode behavior of a gain guided laser device can be remedied by the reduction of the active region's width. Width reduction permits the formation of a substantial number of discrete dielectric levels, which allows for the development of a fundamental mode instead of a multi-mode spectral output, and results in a guided index laser. Both multi-mode and single-

mode devices have been utilized in optical fiber communications systems that can take advantage of their fundamental properties. That is, for multi-mode transmission systems, the multi-mode laser device is used as the optical power source. For single-mode transmission systems, the single-mode optical source is utilized. The implementation of the single-mode optical source in such a transmission system complies with fundamental system design requirements such as low optical modal noise. Laser diodes exhibit a single spectral line with sidelobes reduced by at least 25 dB (Figure 3-23).

In optical fiber communications systems, direct optical modulation of the optical source is an established practice. At very high rates of modulation, the behavior of a single mode optical source begins to change, resulting in an output spectrum that shows more than one spectral line. In order to maintain a single mode spectral output, a modified version of the single-step index laser device is fabricated, that is, a **distributed-feedback laser (DFB)**.

Distributed Feedback Laser Structures

Careful examination of the spectral display of a Fabry-Perot laser diode reveals that it is composed of a central (highest amplitude) modal component and several modal components that have progressively lower amplitudes.

This is a definite disadvantage when used in optical communications systems because its wide spectral width significantly increases chromatic absorption, with a consequent reduction of the usable transmission bandwidth. Ideally, such applications will require a laser diode that exhibits an output spectrum that is composed of a central wavelength component of set amplitude. All the other wavelengths around the center have amplitudes that are significantly reduced.

In DFBs (see Figure 3-24), the main design objective is to generate a single line spectrum at the output, under high data rates of modulation. This is achieved by incorporating a corrugated layer below the active layer of the DFB device. The hills and valleys generate a constant change of the refractive index, which contributes to the device's feedback

mechanism, so that a single mode is produced and undesirable modes are suppressed.

In order for the structure to operate as a DFB device, the grading period must satisfy the relationship exhibited in Equation (3-24).

$$g_P = \frac{\lambda_{\text{mode}}}{n} \quad (3-24)$$

where g_P is the grading period, λ_{mode} is the operating wavelength, and n is the refractive index of the effective mode. Typical operating characteristics of a DFB laser diode are shown in Table 3-1.

DISTRIBUTED BRAGG REFLECTORS. Another single mode feedback laser is the distributed Bragg Feedback device shown in Figure 3-25.

The fundamental structural difference between DFB and DBR lasers is their grading mechanisms. In a DFB device, the grading is at the bottom of the active layer, while in a DBR device the grading is at both ends of the active region. When it is at both ends, it can act as a perfect optical mirror, because of the difference between the constant refractive index of the active layer and the continuously changing refractive index of the grading layer. This structural arrangement provides the required feedback mechanism for optical power generation and spectral purity. DBR devices require a higher threshold current than DFB structures. DBR devices also exhibit a higher degree

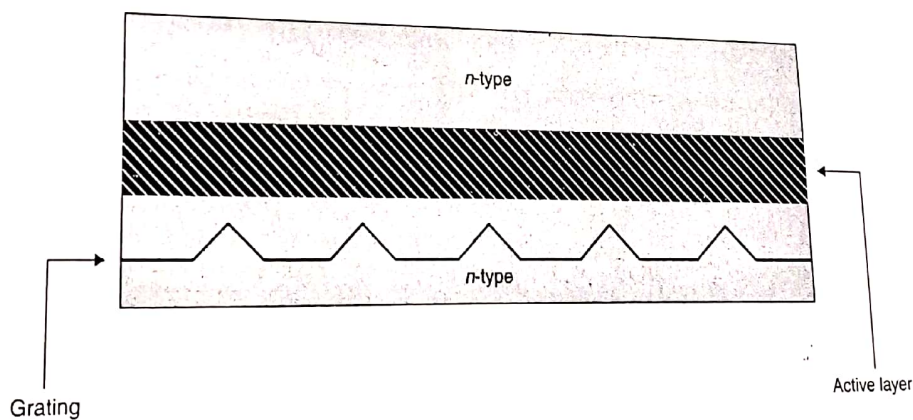


Figure 3-24. Distributed feedback laser.

TABLE 3-1 Typical Operating Characteristics of DFB Lasers

| | |
|---|-----------------------------------|
| Operating wavelength | 1300 nm |
| Output power (max) | $5 \times 10 \text{ mW}$ |
| Threshold current | 40 mA |
| Temperature coefficient (for threshold current) | $1.3 \text{ mA}^{\circ}\text{K}$ |
| Modulation bandwidth | 800 MHz |
| Temperature coefficient | $0.07 \text{ nm}^{\circ}\text{K}$ |
| Spectral bandwidth | 20 MHz |

CHAPTER 3

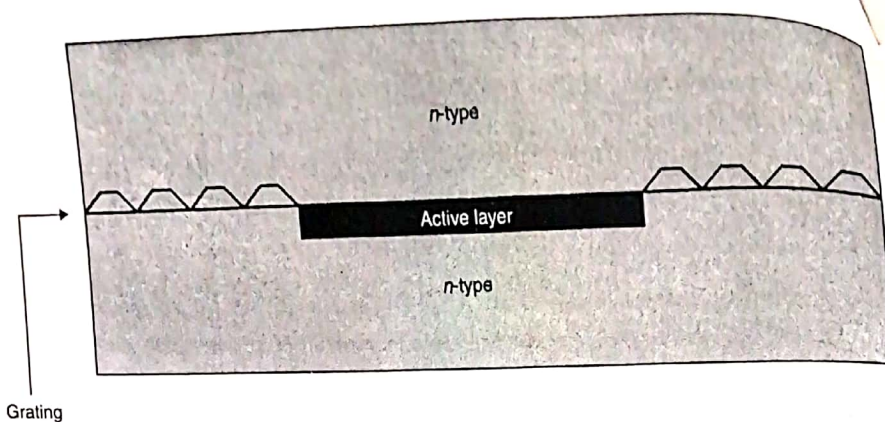


Figure 3-25. A distributed Bragg feedback reflector.

of susceptibility to temperature variations, and their line width is more sensitive to the rate of modulation than DFB laser devices.

LASER DIODE CHARACTERISTICS. There is a spectral difference between gain guided and index guided laser devices. As we mentioned previously, gain guided lasers are multi-mode devices, while index guided lasers are single-mode devices. This is because the spontaneous emission component within index guided structures is smaller than that of the gain guided structure. Under modulated conditions, the single-mode, index guided laser can become a multi-mode device with additional broadening of the modal line width. This is as a result of a small change of the modal frequency, and is attributed to carrier density variations due to pulse modulation. Maintaining a narrow modal line width is crucial when laser devices are used as optical sources for long-distance communications systems that are designed to process high data rates while operating under the most stringent system noise restrictions.

Temperature v. Optical Power

Experimental results have shown that lasers are temperature dependent devices. The relationship of the threshold current and optical power output are subject to operating temperature conditions. This relationship between threshold current and temperature is given by Equation (3-25).

$$I_{th} = I_o e^{\frac{T}{T_o}} \quad (3-25)$$

where I_o is the threshold current at room temperature (characteristic of the laser), I_{th} is the current at operating temperature, T_o is the room temperature (characteristic of the laser device), and T is the operating temperature (characteristic of the laser device).

T_o is an intrinsic value and it is different for GaAs/AlGaAs and InGaAsP/InP laser structure. For example, in InGaAsP devices, T_o has an average value of 65 °K, while for AlGaAs devices, the average T_o is observed to have a value

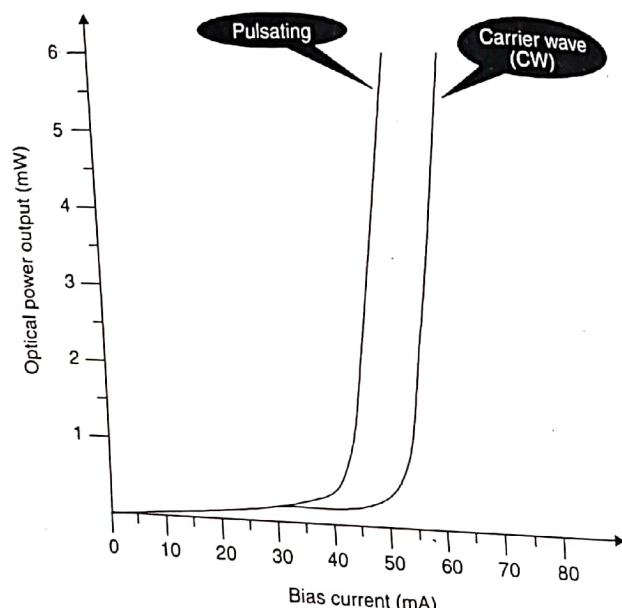


Figure 3-26. Optical power v. biasing current.

of approximately 125 °K. The lower T_o value for InGaAsP devices is attributed to various phenomena occurring inside the device, such as heterobarrier carrier leakage and bond absorption.

When laser diodes are used as optical sources in optical fiber communications systems, the generated output optical power is different for the two basic modes of operations: carrier wave and pulsating. This difference is shown in Figure 3-26.

Figure 3-26 shows that under pulsating modulation, the laser diode requires a smaller threshold current for laser action to take place, while its optical power output is considerably higher in comparison to the carrier wave mode of operation. The threshold current variations v. different operating temperatures are shown in Figure 3-27.

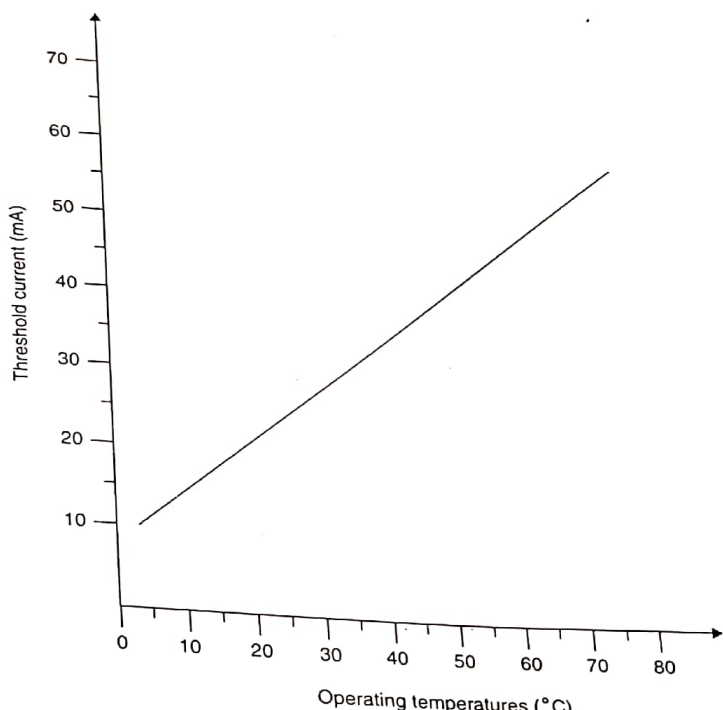


Figure 3-27. Threshold current v. temperature.

Figure 3-27 illustrates a proportional increase of the threshold current in relationship to a corresponding increase of the operating temperature.

These temperature variations also have an effect on the operating wavelength (λ) of the laser device. An increase of 1°C in the operating temperature shifts the operating wavelength by 0.3 nm. This wavelength change is attributed to device cavity expansion due to the increase of the operating temperature.

Laser Bandwidth

One of the fundamental advantages of an optical fiber communications system is its ability to directly modulate the optical source at a very high data rate. Although these modulating rates are very high (approx. 20 GHz), there are limits beyond which the laser diode cannot respond. Figure 3-28 shows the output frequency response of a typical laser diode under modulating conditions.

Figure 3-28 illustrates that under relatively low modulating frequencies, spectral output intensity is constant. When modulating frequency reaches a certain level, the carriers injected into the device cavity interact with the generated photons, enhancing a self-oscillatory process and thus sharply reducing the output spectral density. Another serious problem is **noise intensity**. There is a direct relation-

ship between the noise spectral density and the injected carriers into the active region. The result is an increase of the threshold current beyond the level required for laser action to take place. This spectral noise density is observed to take a maximum value at maximum modulating frequencies. The self-oscillating frequency of a laser device is expressed by Equation (3-26).

$$f_{so} = \frac{1}{2\pi} \sqrt{\frac{AP_o}{\tau}} \quad (3-26)$$

where f_{so} is the self-oscillating frequency, A is the gain, τ is the gain average lifetime of the photon inside the cavity, and P_o is the photon density.

It is evident from Equation (3-26) that in order to increase the range of the oscillating frequency, and consequently to increase the modulation rate and enhance output stability, both photon density and gain must be increased with a simultaneous decrease of the photon (cavity) lifetime. Stabilizing the device operating temperature can be achieved by using a **thermoelectric aperture** (heat sinking), while output power stabilization can be achieved by incorporating a feedback mechanism that can increase the differential gain through a PIN diode. Because the lifetime of photons inside the cavity depends on the physical characteristics of the laser structure, a decrease of the length of the cavity will result in a corresponding decrease

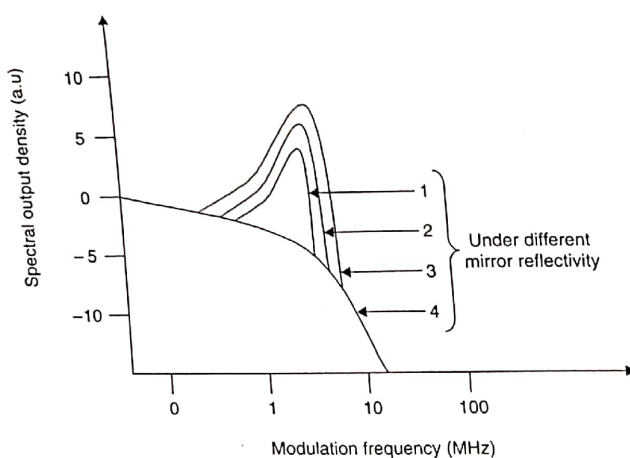


Figure 3-28. Output spectral density v. modulation frequency.

of the (τ). This, of course, has its drawbacks. For example, a decrease in the length of the cavity will increase the carrier density and increase temperature to beyond a certain level.

Laser Device Reliability

Laser devices present a number of challenging problems that result from their fabrication processes. Two common problems are control of the physical dimensions and control of the heterobarrier lattice growth. Various techniques, such as *Liquid Phase Epitaxial (LPE)* growth, have been utilized in the fabrication of laser devices. This technique represents certain difficulties related to uniform reproduction of larger areas. The introduction of the *Vapor Phase Epitaxial (VPE)* growth method has eliminated some of the problems encountered by the LPE fabrication technique. Fabrication techniques, as well as operating conditions, are key factors in determining a device's reliability and life span. Both these factors are very important when the optical device is considered for utilization in an optical fiber communications system. The operating life span of an optical source is the period for which the device is capable of delivering specified optical power at a predetermined maximum threshold current. Over time, internal degradation based on operating temperatures, crystal defects, facet, and conduct damages limit a device's life span.

3.4 QUANTUM WELL LASER DIODES

The basic objective in the design of laser diodes is to obtain the highest optical gains at the lowest possible carrier densities, ultimately reflecting much lower threshold current requirements. Conventional double heterojunction laser diodes are unable to fully satisfy performance requirements because of the relatively thick active layer. If the active layer is divided in sublayers with widths of the order of a few

nanometers, while separated by equally thin barrier layers, then the carrier movement across the individual thin active layers will be somewhat restricted and the kinetic energy will appear to be quantized to discrete energy levels. Because of the transformation of the forward kinetic energy to quantum energy levels in the active region, these devices are referred to as quantum well (QW) laser diodes. The energy bands of such a structure are illustrated in Figure 3-29.

Figure 3-29 illustrates the optical spectrums of four single quantum well (SQW) laser diodes with different active layer thicknesses. It also illustrates a slight peak wavelength shift at an active layer thickness of less than 17 Å°.

The discrete energy states within the active region alter the optical and electronic properties of the beam, promoting higher optical gains at much lower threshold currents in comparison to double heterojunction laser diodes.

Multi Quantum Well Laser Diodes

To further enhance laser diode operating performance, the quantum well concept was extended beyond the SQW concept, to a new semiconductor structure incorporating more than one quantum well, referred to as multi quantum well laser diodes (MQW). The energy bands of an MQW diode are illustrated in Figure 3-30.

MQW lasers employ a multilevel active region that is separated by barrier layers. In such a device, the barrier energy level and the cladding energy level are equal. A different energy level between the barrier and the cladding layers results in a modified version of the MQW structure, referred to as a modified multi quantum well laser diode (M-MQW). M-MQWs have no significant changes in their performance characteristics.

QW semiconductor structures allow carrier energy states to be elevated above the band gap level by confining the carriers in quantum wells within the active layer in a super lattice

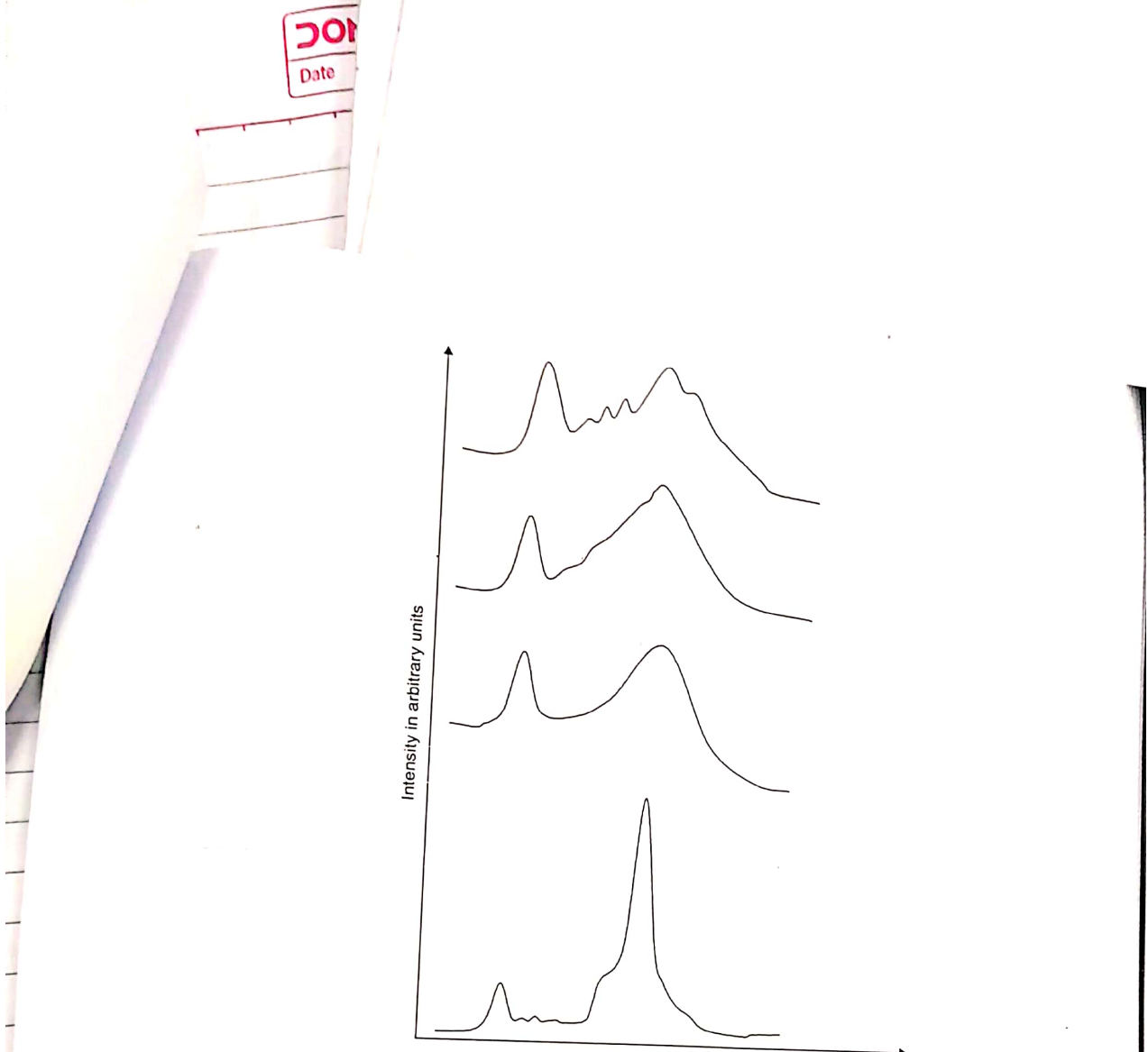


Figure 3–29. Energy band levels of single quantum well laser structures composed of four different well sizes.

structure. Laser action can be initiated by employing radiative transitions among the confined carriers in the quantum wells.

MQW lasers are fabricated from nitride materials grown on MgAlO substrates. These materials exhibit characteristics such as high thermal conductivity, very large heterojunction offsets, high melting temperatures, and physical hardness. That is, an InGaN MQW active layer is sandwiched between two GaN optical guides and AlGaN cladding layers. Multi quantum well technology is today applied in the fabrication of both LED and laser diode devices that operate at very short wavelengths, down to the 410 nm range.

InGaN compounds that have direct bandgaps between 1.95 eV and 3.4 eV at room temperature can be used as active layers in MQW LED and laser diode structures that operate in the blue wavelength region. Figure 3–31 illustrates a cross section of an MQW laser diode.

The device in Figure 3–31 is capable of emitting at very short wavelengths (~400 nm), the shortest ever achieved by a semiconductor laser diode. For Figure 3–31, a buffer layer of GaN is grown on a $MgAl_2O_4$ substrate. The active region is composed of an InGaN MQW layer (20-periods), the emitting light from which is confined by a *p*-type and *n*-type AlGaN guiding layer, while *n*-type InGaN is used as buffer to protect the AlGaN from damaging the very thin film. The *p*-type AlGaN is used to maintain the bond between the InGaN layers of GaN is used to maintain the bond between the InGaN layers of

the active region during the *p*-type layer growth process. The *p*-type and the *n*-type GaN on both sides of the active region are functioning as light guiding layers. The electrical characteristics of an InGaN MQW device is illustrated in Figure 3–32 (see page 87).

Figure 3–32 illustrates InGaN MQW laser diode polarized output intensity versus a pulse modulated biasing current. Close examination of Figure 3–32 shows that for a biasing current of 300 mA, no stimulation of emission is observed. At 310 mA, stimulation of emission begins to form (threshold current), and at 400 mA of biasing current, a maximum optical power output of 35 mW is obtained. Figure 3–33 (see page 87) illustrates the optical spectrums of an InGaN MQW laser diode for three different biasing current levels.

Line (a) illustrates the optical spectrum of a laser diode at a biasing current level of 0.6 A. The measured full wave at half maximum (FWHM) is 22 nm. The optical output power is the result of the spontaneous emission of radiation and it peaks at ~404 nm wavelength. Line (b) illustrates the optical spectrum at a biasing current of 1.2 A. The peak wavelength has been shifted to 410 nm and the optical power output (much higher), indicates the starting of the stimulation of emission process. Line (c) illustrates the optical spectrum at a biasing current above the threshold level. It is evident that the FWHM is approximately 1/10 (21 nm) that of line (a).

3.5 SURFACE EMITTING LASERS

The ever-increasing demand for higher transmission capacities, longer distances between amplification, optical interconnections, and optical computing generated the incentive for the development of surface emitting lasers (SEL). SELs are classified into four major categories:

- i) Vertical Cavity Surface Emitting Lasers (VCSEL)
- ii) Folded Cavity (FCSEL)
- iii) 45°C Reflecting Mirror (45°C-RMSEL)
- iv) Grating Coupled (GCSEL)

The fundamental advantages of SELs are that they can be massively fabricated by monolithic processing, they are able to vertically harvest the generated optical power, and they are able to be tested and have their performance evaluated before separated in individual devices. The fact that they can be fabricated in large numbers of arrays leads to the generation of relatively high optical laser power (Figure 3-34, see page 88).

3.6 VERTICAL CAVITY SURFACE EMITTING LASERS

The fundamental difficulty with standard SEL diodes lies in their inability to operate at room temperature because of short gain path relevant to insufficient mirror reflectivity. To improve the p -side mirror reflectivity, a ring electrode was introduced, while on the n -side, a multilayer reflector was introduced to improve mirror reflectivity. However, in order to improve the second important performance parameter (that is, the substantial reduction of the threshold current (I_{th})), a thin circular heterostructure active layer was induced in the optical confinement waveguide. The first CW-VCSEL diode operating at room temperature was fabricated in 1988, and was composed of GaAlAs/GaAs compounds. By 1989, CW-VCSEL diodes lasing at 2 mA threshold current at room temperature were realized. Full commercial applications of such diodes began in early 1996. A three dimensional visualization of a VCSEL diode is illustrated in Figure 3-35 (see page 88).

Figure 3-35 shows the active layer embedded in a smaller bandgap material. Therefore, the injected carriers are confined within the active region. The surface area of the active region πD^2 defines the base of the cylindrical vertical waveguide. In order for the optical of a dominant mode to be detected at the output of the cylindrical waveguide, the modal gain must be at least equal to the total optical losses. The relationship between the modal gain and the optical losses is expressed by Equation (3-27).

$$KG_{th} = (\alpha_m + \alpha_T) \quad (3-27)$$

where K is the optical energy confinement factor, G_{th} is the modal gain at threshold current, α_m represents mirror

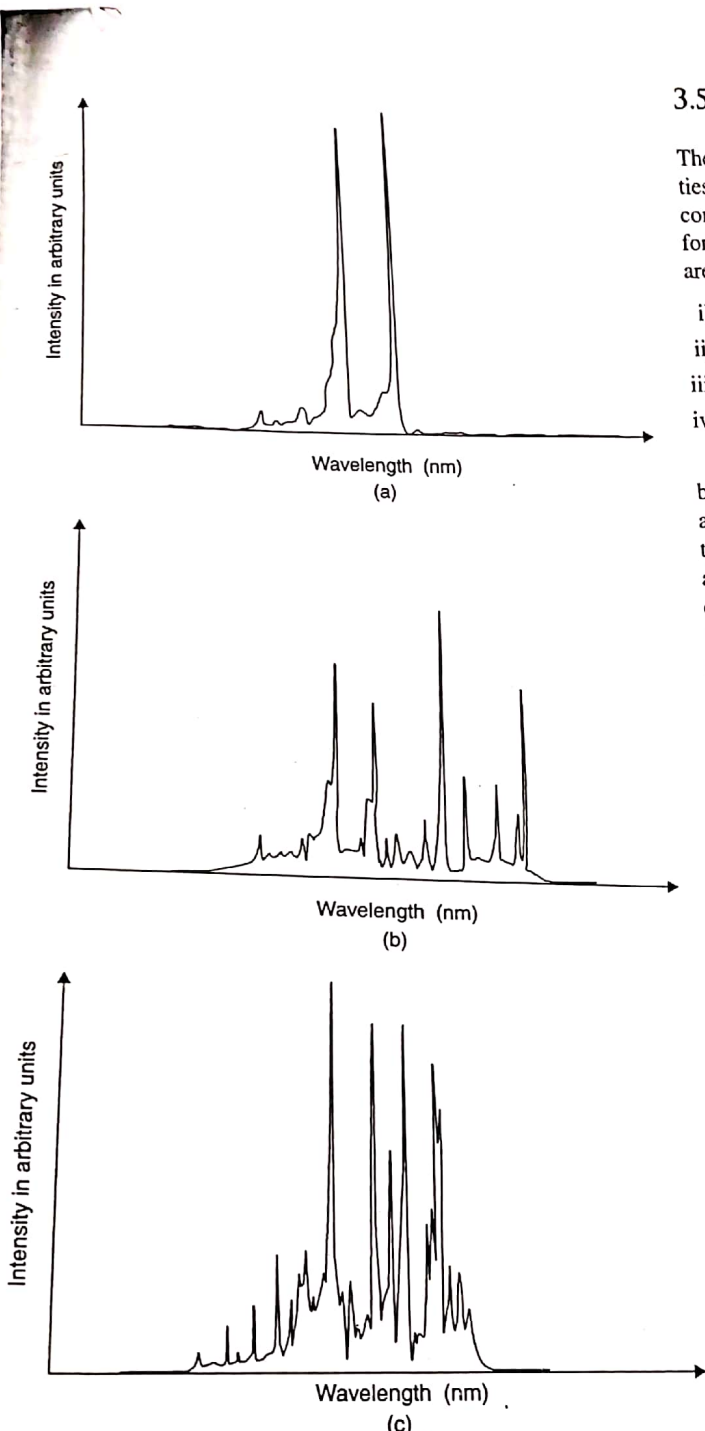
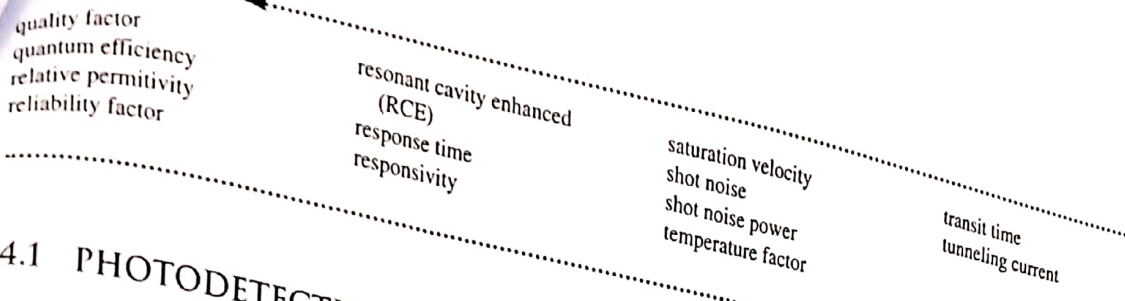


Figure 3-30. Energy band levels of MQW laser structure for different biasing current levels.

InGaN MQW laser diodes exhibit very low FWHM and high optical output power at very low operating wavelengths. A decrease of the thickness of the active layer will further shift the operating wavelengths. If the emission energy increases, the FWHM will also increase, resulting in a corresponding decrease of quantum well luminescence.



4.1 PHOTODETECTION

Photodetection is the process whereby optical power is detected and then converted to electrical power. Photodetector devices (optical detectors) perform photodetection. Optical detectors perform the opposite function of that of optical sources: they convert electric power into optical power.

In any optical fiber communications system, the optical source is part of the transmitter section, while optical detectors are part of the receiver section. The performance of an optical detector incorporated into the receiver section of an optical fiber communications system can be determined by its ability to detect the smallest optical power possible (detector sensitivity) and generate a maximum electric power at its output with an absolute minimum degree of distortion (low noise). Optical detectors must also exhibit a comparatively wide bandwidth and sharp response to accommodate the high bit-rate required by such a system. Other criteria for selecting a particular photo diode for implementation into an optical fiber communications system are the ability to interface with optical cables, a long operating life, and cost.

Although there are several types of photodetectors, not all of them are suitable for use in optical fiber communications systems. In such systems, the optical detector device, which is almost always utilized, is the semiconductor photodiode.

Photodetector design criteria are set forth by system parameters such as size, sensitivity, bandwidth, and degree of tolerance to temperature variations.

The two photodetector devices most commonly used in optical fiber communications systems are PIN and APD devices.

4.2 PIN PHOTODETECTORS

The principal theory on which a P-region, I-intrinsic, n-region (PIN) photodetector device is based is illustrated in Figure 4-1.

When a photon is incident upon a semiconductor photodetector device, and it has more energy than the band gap energy of that device, the energy of the photon is absorbed by the band gap and an electron-hole pair is generated across the band gap. The energy of the incident photon is given by Equation (4-1).

$$E_{ph} = \frac{hc}{\lambda} \quad (4-1)$$

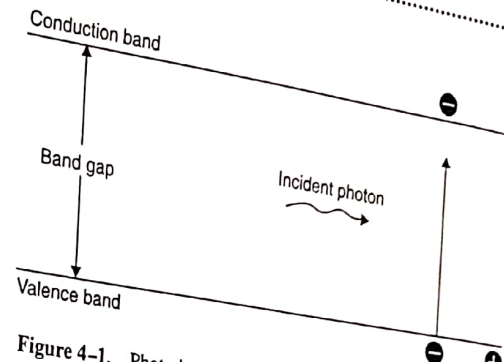


Figure 4-1. Photodetector device.

where E_{ph} is the energy of the photon, h is Planck's constant ($6.62 \times 10^{-34} \text{ Js}^2$), c is the velocity of light ($3 \times 10^8 \text{ m/s}$), λ is the wavelength (m), E_g is the band gap energy.

It is evident from Equation (4-1) that the photon energy (E_{ph}) is inversely proportional to the wavelength (λ). Therefore, a wavelength, at which the photon energy becomes equal to the band gap energy, exists. At this photon energy level, electron-hole generation will occur. The wavelength at which the photon energy becomes equal to band gap energy is called the cut off wavelength (λ_c). From Equation (4-1), solving for (λ) we have Equation (4-2).

$$\lambda = \frac{hc}{E_{ph}}$$

Because $E_{ph} = E_g = eV$

$$\text{then } \lambda = \frac{hc}{E_g}$$

Substituting for: h ($6.62 \times 10^{-34} \text{ Js}^2$)
 c ($3 \times 10^8 \text{ m/s}$)

Therefore,

$$\lambda_c = \frac{1.24 \mu\text{m}}{E_g} \quad (4-2)$$

Semiconductor materials employed in the fabrication of photodetectors are the same with the materials employed in the fabrication of optical sources.

Each individual element or substance is classified by a band gap energy level (E_g) characteristic of that element or substance. Therefore, different materials exhibit different cut off wavelengths. Some materials, with their corresponding band gap energy levels (eV), are listed in Table 4-1.

Applying these energy gap levels to Equation (4-2) yields the following cut off wavelengths.

$$\text{For Ge: } \lambda_c = \frac{1.24}{0.67} = 1.85 \mu\text{m}$$

TABLE 4-1 Band Gap Energy Levels

| Elements/Substances | | Band Gap Energy (eV) |
|------------------------------------|---------|----------------------|
| Germanium | Ge | 0.67 |
| Silicon | Si | 1.11 |
| Indium gallium arsenide | InGaAs | 0.77 |
| Indium gallium arsenide phosphorus | InGaAsP | 0.89 |

Therefore, the cut off wavelength for Ge is 1.85 μm .

$$\text{For Si: } \lambda_c = \frac{1.24}{1.11} = 1.11 \mu\text{m}$$

Therefore, the cut off wavelength for Si is 1.11 μm .

$$\text{For InGaAs: } \lambda_c = \frac{1.24}{0.77} = 1.61 \mu\text{m}$$

Therefore, the cut off wavelength for InGaAs is 1.61 μm .

$$\text{For InGaAsP: } \lambda_c = \frac{1.24}{0.89} = 1.4 \mu\text{m}$$

Therefore, the cut off wavelength for InGaAsP is 1.4 μm .

A cross section of a silicon PIN diode is shown in Figure 4-2. When a photon enters the photodetector, the low band gap absorption layer absorbs the photon, and an electron-hole pair is generated. This electron-hole pair is called a photocarrier.

These photocarriers, under the influence of a strong electric field that was generated by a reverse bias potential difference across the device, are separated and form a photo-current intensity proportional to the number of incident photons. The DC biasing of a PIN diode photo detector is shown in Figure 4-3.

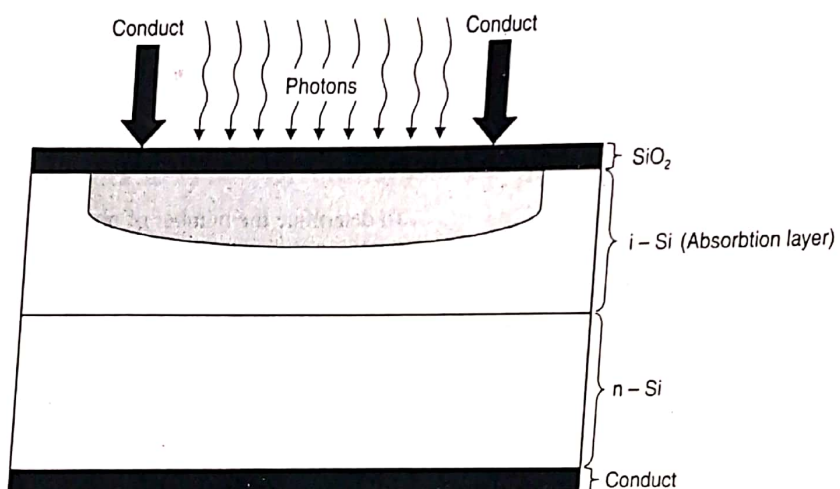


Figure 4-2. A cross section of a silicon PIN diode.

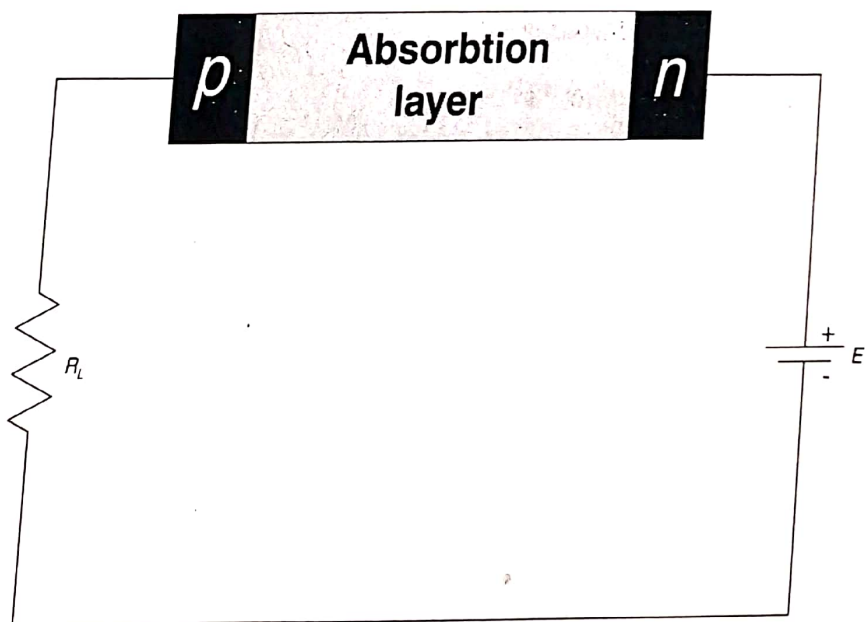


Figure 4-3. Diode biasing.

1.61 μm

The photocurrent generated from the PIN photodetector device develops a potential difference across the load resistance (R_L), with a frequency calculated as follows in Equation (4-3).

$$f = \frac{E_{ph}}{h} \quad (4-3)$$

where E_{ph} is the photon energy (eV), h is Planck's constant $6.62 \times 10^{-34} \text{ Js}^2$, and f is the frequency. Because a cut off wavelength for each substance used in the fabrication of a PIN photodetector exists, a cut off frequency for each element or substance also exists. The cut off frequency can be calculated as follows.

$$\text{For Ge: } f_c = \frac{E_{ph}}{h}$$

First, the E_{ph} must be converted from eV to Joules: $1 \text{ eV} = 1.6 \times 10^{-19} \text{ J}$

For germanium, $\text{Ge} = 0.67 \text{ eV}$

In Joules, $1.6 \times 0.67 \times 10^{-19} \text{ J} = 1.07 \times 10^{-19} \text{ J}$

$$f_c = \frac{1.07 \times 10^{-19} \text{ J}}{6.62 \times 10^{-34} \text{ Js}^2} = 161 \times 10^{12} \text{ Hz}$$

Therefore, the cut off frequency for Ge is 161 THz.

For silicon, $\text{Si} = 1.11 \text{ eV}$.

In Joules, $1.11 \times 1.6 \times 10^{-19} \text{ J} = 1.776 \times 10^{-19} \text{ J}$

$$f_c = \frac{1.776 \times 10^{-19} \text{ J}}{6.62 \times 10^{-34} \text{ Js}^2} = 268 \times 10^{12} \text{ Hz}$$

Therefore, the cut off frequency for Si is 268 THz.

For indium gallium arsenide, $\text{InGaAs} = 0.77 \text{ eV}$.

In Joules, $0.77 \times 1.6 \times 10^{-19} \text{ J} = 1.232 \times 10^{-19} \text{ J}$

$$f_c = \frac{1.232 \times 10^{-19} \text{ J}}{6.62 \times 10^{-34} \text{ Js}^2} = 186 \times 10^{12} \text{ Hz}$$

Therefore, the cut off frequency for InGaAs is 186 Thz.

For indium gallium arsenide phosphorus, $\text{InGaAsP} = 0.89 \text{ eV}$.

In Joules, $0.89 \times 1.6 \times 10^{-19} \text{ J} = 1.424 \times 10^{-19} \text{ J}$

$$f_c = \frac{1.424 \times 10^{-19} \text{ J}}{6.62 \times 10^{-34} \text{ Js}^2} = 215 \times 10^{12} \text{ Hz}$$

Therefore, the cut off frequency for InGaAsP is 215 THz.

The combination of different semiconductor alloys that are all operating at different wavelengths allows the selection of material capable of responding to the desired operating wavelength. For example: GaAs/AlGaAs substances operate at wavelengths between 800 nm and 900 nm, while photodetector devices composed of InGaAs/InP alloys operate at wavelengths between 1000 nm and 1600 nm.

PIN Photodetector Characteristics

The fundamental PIN photodiode operational characteristics are quantum efficiency (η), responsivity (R), speed, and linearity.

Quantum efficiency (η) is defined by the number of electron-hole pairs generated per photon (Equation (4-4)).

$$\eta = \frac{N(e^-, p^+)}{N_{ph}} \quad (4-4)$$

where $N(e^-, p^+)$ is the number of generated electron-holes, N_{ph} is the number of photons, and η is the quantum efficiency. The number of generated electron-hole pairs is translated to current by using Equation (4-5).

$$I_p = q \times N_e^- \quad (4-5)$$

To determine the number of electrons, solve Equation (4-5) for N_e^- , yielding Equation (4-6).

$$N_e^- = \frac{I_p}{q} \quad (4-6)$$

where I_p is the photocurrent (mA), q is the electron charge ($1.6 \times 10^{-19} \text{ C}$), and N_e^- is the number of electrons. Consequently, the number of incident photons is translated to light power through Equation (4-7).

$$P_o = N_{ph} \times h\nu \quad (4-7)$$

To determine the number of photons, solve Equation (4-7) for N_{ph} , yielding Equation (4-8).

$$N_{ph} = \frac{P_o}{h\nu} \quad (4-8)$$

where P_o is the light power, N_{ph} is the number of photons, h is Planck's constant ($6.626 \times 10^{-38} \text{ J/s}$), v is the velocity of light, and λ is the wavelength.

Substituting Equations (4-6) and (4-8) into Equation (4-4) yields Equation (4-9).

$$\eta = \frac{N_e^-}{N_{ph}} = \frac{\frac{I_p}{q}}{\frac{P_o}{h\nu}} = \frac{I_p h\nu}{q P_o}$$

Substituting for $v = \frac{c}{\lambda}$,

$$\eta = \frac{I_p hc}{q P_o \lambda}$$

Because $E_{ph} = \frac{hc}{\lambda}$,

$$\text{therefore, } \eta = \frac{I_p E_{ph}}{q P_o} \quad (4-9)$$

From the quantum efficiency equation, it is evident that the efficiency of a PIN photodetector is proportional to the photon energy absorbed by the absorption layer of the device. Larger photon energy requires a thicker absorption

layer, allowing longer time for electron-hole pair generation to take place.

Response Time (Speed)

Response time or speed of a photodetector is referred to as the time required by the generated carriers within the absorption region to travel that region under reverse bias conditions.

The main factor that determines this time is the thickness of the absorption region. The thicker the absorption region, the longer the time. Here, there is a conflict between photodetector efficiency and response time. For higher efficiency, a thicker absorption region is needed, while for higher speed, a thinner absorption region is required. In practice, trade-offs between efficiency and speed are made to accommodate design objectives. The response time (t_r) of a photodetector is given by the relationship

$$t_r = \frac{\text{thickness of the absorption layer}}{\text{saturation velocity}}$$

Saturation velocity (V) for a typical InGaAs alloy is 10^7 m/s. Given the device absorption layer thickness, the response time can be calculated.

Example 4-1

Compute the response time of PIN photodetector composed of InGaAs with 5 μm of absorption layer thickness.

Solution

$$t_r = \frac{5 \times 10^{-6} \text{ m}}{1 \times 10^7 \text{ m/s}} = 5 \times 10^{-13} \text{ s}$$

or $t_r = 0.5 \text{ ps}$.

The key parameter for determining photodetector device performance is responsivity. Responsivity is defined

by the ratio of the current generated in the absorption region per-unit optical power incident to the region. Responsivity is closely related to quantum efficiency and is expressed by Equation (4-10).

$$R = \eta \frac{q}{E_{ph}} \quad (4-10)$$

where R is the responsivity, η is the quantum efficiency, q is the electron charge ($1.59 \times 10^{-19} \text{ C}$), and E_{ph} is the energy of the photon (hv). Substituting Equation (4-4) (quantum efficiency) into Equation (4-10) yields Equation (4-11).

$$R = \frac{I_p E_{ph}}{P_o} \times \frac{q}{E_{ph}} = \frac{I_p}{P_o}$$

Therefore,

$$R = \frac{I_p (\mu\text{A})}{P_o (\mu\text{W})} \quad (4-11)$$

The responsivity of a PIN photodiode is the ratio of the generated photocurrent per incident of unit-light power.

A graphical representation of quantum efficiency (η) and responsivity is shown in Figure 4-4.

Figure 4-4 illustrates the fundamental difference between responsivity and quantum efficiency. For different semiconductor materials, the responsivity is linear up to a particular wavelength, then it drops quickly. Beyond this point, the photon energy becomes less than the energy required for electron-hole generation.

Dark Current

Dark current (I_d) is defined as the reverse leakage current of a photodetector device in the absence of optical power entering the photodetector device. Dark current is an unwanted element caused by factors such as current recom-

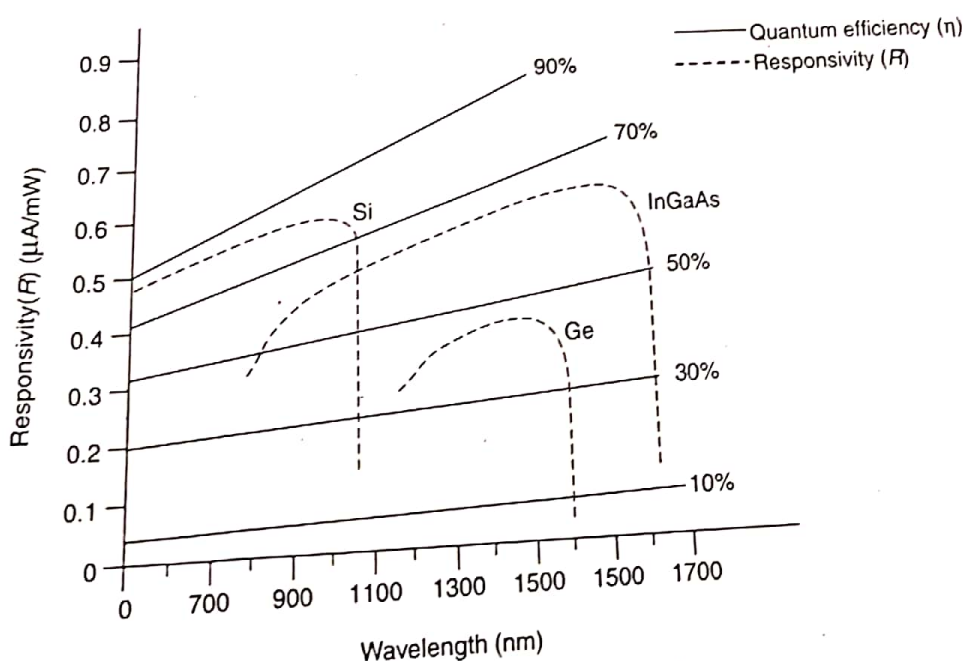


Figure 4-4. A graphical representation of quantum efficiency (η) and responsivity (R) in reference to operating wavelength.

combination within the depletion region and surface leakage current. The negative effects of such unwanted currents contribute to thermal shot noise first observed by W. Schottky. While experimenting with vacuum tubes he observed that certain spontaneous fluctuations of the DC anode current were periodically occurring. Further observations and studies concluded that these fluctuations were the result of the particle nature of free electrons moving randomly under the influence of a potential difference applied across the anode and the cathode of the tube.

Shot Noise

In semiconductor devices, shot noise is the result of electron-hole recombination and majority carrier random diffusion. The power spectral density of shot noise is proportional to the dark current and is expressed by Equation (4-12).

$$P_n = 2I_d q B_w \quad (4-12)$$

where P_n is the shot noise power (W), I_d is the dark current (A), q is the electron charge ($1.59 \times 10^{-19} C$), and B_w is the operating bandwidth. Shot noise-voltage (V_n) is expressed by Equation (4-13).

$$V_n = 2I_d q B_w \quad (4-13)$$

where V_n is the noise voltage and B_w is the receiver operating bandwidth.

Thermal (Johnson) Noise

Thermal noise is the result of thermally agitated free-electron motion within any conducting material. Thermally agitated electrons within a conductor collide with the molecules of that conductor, thus starting a chain reaction with all other free electrons. The average of thermal noise is zero, at which point the material is said to be in thermal equilibrium. Therefore there is no DC component. The voltage probability is Gaussian with a mean square voltage given by Equation (4-14).

$$V_n = 4KT \int_{f_1}^{f_2} R(f) P(f) df \quad (4-14)$$

$P(f)$ is defined as follows in Equation (4-15).

$$P(f) = \frac{hf}{KT} (e^{-hf/RT} - 1)^{-1} \quad (4-15)$$

where T is the absolute temperature ($290^\circ K$), K is Boltzmann's constant ($1.38 \times 10^{-23} J/K$), f is the frequency (Hz) (bandwidth of the observed voltage), h is Planck's constant ($6.62 \times 10^{-34} J/s$), and R is the impedance (Ω). For a temperature of $T = 290^\circ K$ and frequency $f \geq 100 \text{ GHz}$, $P(f)$ takes a value between 0.992 and 1 ($0.992 < P(f) < 1$); therefore, $P(f) \approx 1$ and noise voltage becomes Equation (4-16).

$$V_n = \sqrt{4KT B_w R} \quad (4-16)$$

The thermal noise power $P_{n(\text{thermal})}$ is expressed by Equation (4-17).

$$P_{n(\text{thermal})} = KTB_w \quad (4-17)$$

Shot-noise-voltage (V_n) is expressed by Equation (4-18), which is the same as Equation (4-13).

$$V_n = 2I_d B_w \quad (4-18)$$

where V_n is the noise voltage and B_w is the receiver operating bandwidth.

Signal to Noise Ratio

The signal to noise ratio (SNR) expresses (in decibels) the difference between the signal power and noise power at the input or output of an electronic device or circuit. This ratio is perhaps the most important criteria used to establish the performance of electronic devices or circuits. The SNR redundant is given by Equation (4-19).

$$SNR_{ab} = 10 \log \frac{P_s}{P_n} \quad (4-19)$$

where P_s is the power of the signal (W) and P_n is the power of the noise (W) (total noise power). Based on Equation (4-19), the SNR can be thought of as the logarithmic ratio of the signal power to the sum total of the noise power (shot noise and thermal or Johnson noise).

Equation (4-13) indicates that an increase of dark current will decrease the overall receiver operation bandwidth by maintaining a constant noise voltage level. Although it can be reduced considerably by proper material selection and controlled fabrication techniques, the dark current cannot be totally eliminated. This unwanted current is also temperature dependent. That is, it increases with an increase in the operating temperature. Therefore, proper control of materials fabrication techniques and operating temperatures are key factors for the reduction of dark current and, consequently, for enhancing the operating performance of the PIN photodetector device.

4.3 AVALANCHE PHOTODETECTORS

Avalanche photodetectors (APD) are very similar to PIN diodes, with only one exception: the addition to the APD device of a high intensity electric field region. In this region, the primary electron-hole pairs generated by the incident photons are able to absorb enough kinetic energy from the strong electric field to collide with atoms present in this region, thus generating more electron-hole pairs. This process of generating more than one electron-hole pair from one incident photon through the ionization process is referred to as the avalanche effect.

It is apparent that the photocurrent generated by an APD photodetector device exceeds the current generated by a PIN device by a factor referred to as the multiplication factor (M).

Because the current generated by a PIN device is expressed as $I = qN_{e^-}$, the generated photocurrent is expressed by Equation (4-20).

$$I_p = (qN_{e^-})M \quad (4-20)$$

where I_p is the generated photocurrent, q is the electron charge ($1.59 \times 10^{-19} \text{ C}$), N_{e^-} is the carrier number, and M is the multiplication factor. The multiplication factor depends on the physical and operational characteristics of the photodetector device. Operational characteristics include the width of the avalanche region, the strength of the electric field, and the type of semiconductor material employed. The cross section of a short wavelength silicon APD device is shown in Figure 4-5. This structure is composed of a $p^+ - p^- - pn^+$ semiconductor material. A light doped p^- region is epitaxially grown on a heavily doped p^+ -type substrate.

When a reverse biased voltage is gradually applied across the diode, an electric field develops across the avalanche region. Its strongest intensity is measured at the pn^+ junction. As the reverse biasing voltage gradually increases, the corresponding electric field across the region also increases and, as a consequence, there is an expansion of the depletion region. If the electric field intensity increases just below the avalanche breakdown point, the depletion region has almost reached the total width of the p^- layer. Under these circumstances, if a photon is incident upon the device, it will be absorbed by the p^- layer. The energy released by the incident photon causes the generation of the first electron-hole pair. Under the influence of the strong electron field, the generated electron is guided from the p^- intrinsic region closer to the pn^+ junction. At this point, the electric field intensity is at its maximum.

Under the influence of the strong electric field, the entering electron collides with other atoms, thus generating a new electron pair. The secondary electron, still under the

influence of the strong electric field, generates another electron-hole pair, and so on (avalanche effect).

The number of the secondary electron-hole pairs that are generated is proportional to the carrier distance traveled through the avalanche region and to the semiconductor materials used for the fabrication of photodetector devices. Figure 4-6 shows the relationship between electric field strengths, and ionization rates for different alloys employed in the fabrication of photodetector diodes.

The equivalent circuit of an avalanche-photodetector diode is shown in Figure 4-7. When reverse biased, an electronic field develops across the depletion region with its maximum field strength across the $p-n$ junction. The avalanche effect will occur only when the depletion region has reached its maximum or is fully developed.

A cross section of an InGaAs photodetector device is shown in Figure 4-8. This is a double heterostructure device incorporating an InGaAs low bandgap absorption layer, while the InP is used as a confinement layer with a band gap higher than that of the absorption layer. This higher band gap of InP ensures that no photon absorption will occur in the confinement layer.

One of the fundamental operating characteristics of a photodetector device is its available bandwidth. The number of holes present in the device limits available bandwidth. The InGaAP layer is epitaxially grown on the absorption layer with a band gap somewhere between the absorption and confinement layers. This arrangement removes the bandwidth limiting holes, and thus enhances the overall bandwidth characteristics of the photodetector device. The absorption layer is elevated to a higher band gap region, resulting in the first electron-hole pair generated by the incident photon. The generated electron under the influence of the very strong electric field is guided to the p^- InP ring. At the pn^+ junction, the electric field is at maximum, with a maximum depletion region. Through this region, impact ionization takes place, resulting in photocurrent multiplication. Another basic performance characteristic of an APD photodetector device is the ratio of the electron and hole ionization rates to the different semiconductor materials used during the fabrication process. This electron-hole ionization ratio is a key factor, as it determines gain bandwidth product and noise performance characteristics. For example, let us suppose that electrons are the primary carriers in an APD structure. A higher electron-to-hole ratio reflects a low noise and higher gain bandwidth product, while a low electron-to-hole ratio reflects a higher noise and lower gain bandwidth product.

Gain

The photocurrent gain in an APD device is a function of several elements such as: the wavelength of the incident photons, the electric field strength as a result of the reverse bias voltage, the width of the depletion region, and the types of semiconductor materials used for the fabrication of the APD device. The relationship of the photocurrent gain to biasing

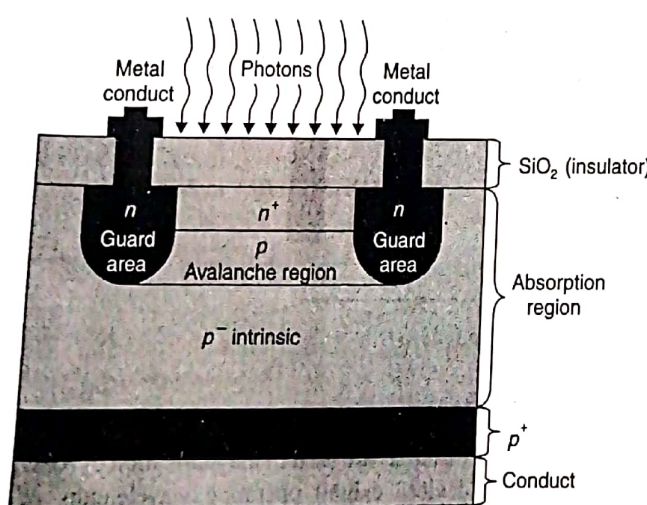


Figure 4-5. Silicon APD device.



generates another
n-hole pairs that
instance traveled
semiconductor
ctor devices.
electric field
employed
detector
n elec-
th its
ava-
has

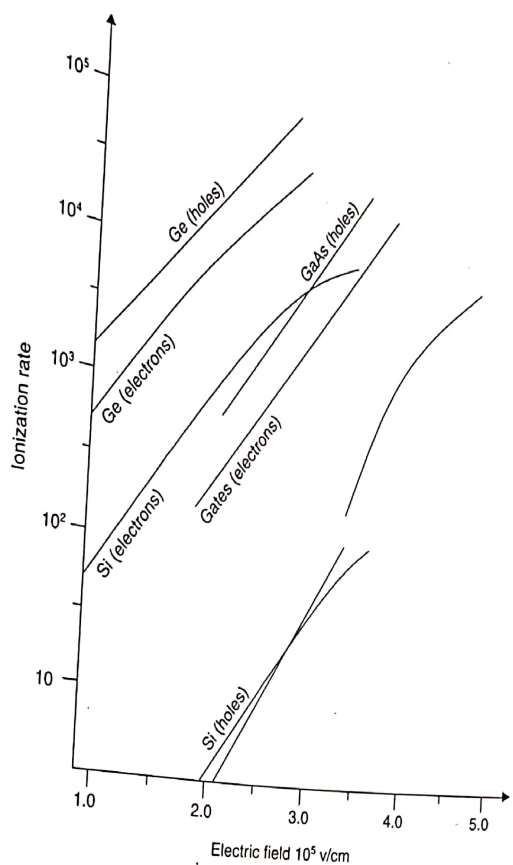


Figure 4-6. Ionization rate v. electric field strength for various alloys.

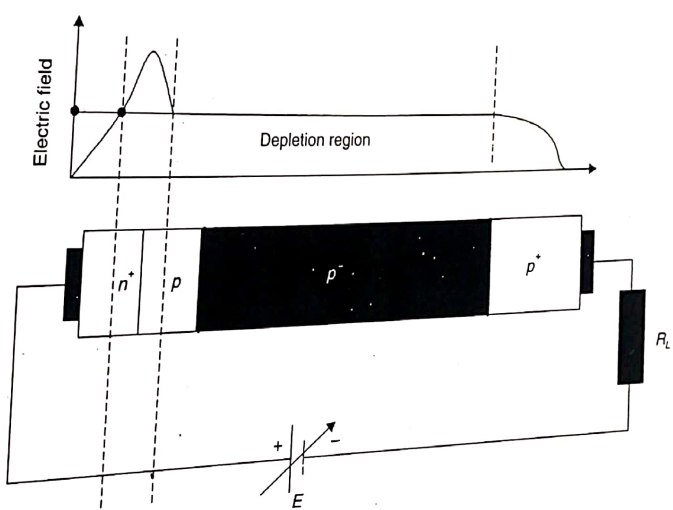


Figure 4-7. Equivalent circuit for APD (minimum electric field required for avalanche effect).

voltage for different wavelengths is shown in Figure 4-9. It is evident that higher photocurrent gain is observed at higher wavelengths at specific reverse biasing voltages.

The function of the guard rings in an APD structure is to prevent edge breakdown around the avalanche region.

When InGaAsP materials are used in the fabrication of APD devices, these devices exhibit operating wavelengths of between 900 nm and 1600 nm; when silicon materials are used, they exhibit operating wavelengths of between 400 nm and 900 nm.

CHAPTER 4

temperature, and α is the factor determining temperature graphs.

Photodetector Noise

Avalanche photodetectors exhibit higher noise than PIN devices. This is a result of the ionization multiplication process that takes place in the device. The random nature of the current multiplication results in a random output of the device, and can be described by the equation:

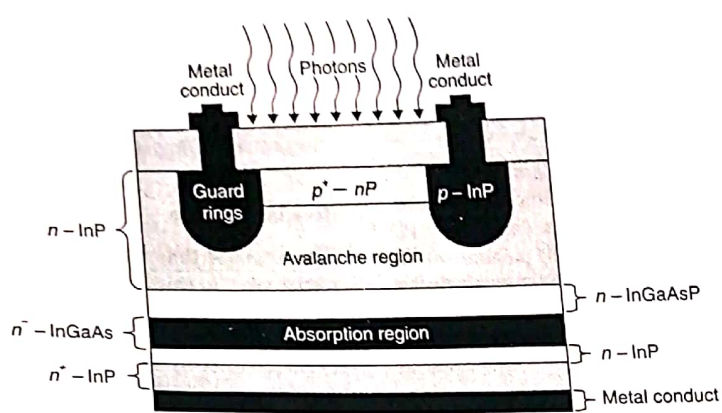


Figure 4-8. A cross section of an InGaAs photodetector device.

Photocurrent gain, an important parameter of an APD device, is also temperature dependent. Figure 4-10 shows an increase of the multiplication factor with a corresponding increase in the operation temperature at a constant reverse biasing voltage. Current fluctuation with temperature is an undesirable phenomenon and must be confined to a tolerable level or completely eliminated. To maintain a constant multiplication factor for a wide range of operating temperatures, any increase in the generated photocurrent due to an increase in the operating temperature must be compensated for by a proportional decrease of the reverse biasing voltage. The equation that determines

the (current-gain) multiplication factor (M), in reference to reverse biasing voltage and operating temperature, is given by Equation (4-21).

$$M = \frac{1}{1 - \left[\frac{V_a - I_p R_L}{V_{BK} [1 + \alpha(T_1 - T_o)]} \right]} \quad (4-21)$$

where V_a is the reverse biasing voltage (V), I_p is the multiplied photocurrent (mA), R_L is the device resistance plus load resistance, V_{BK} is the breakdown voltage at room temperature, T_o is the room temperature, T_1 is the operating

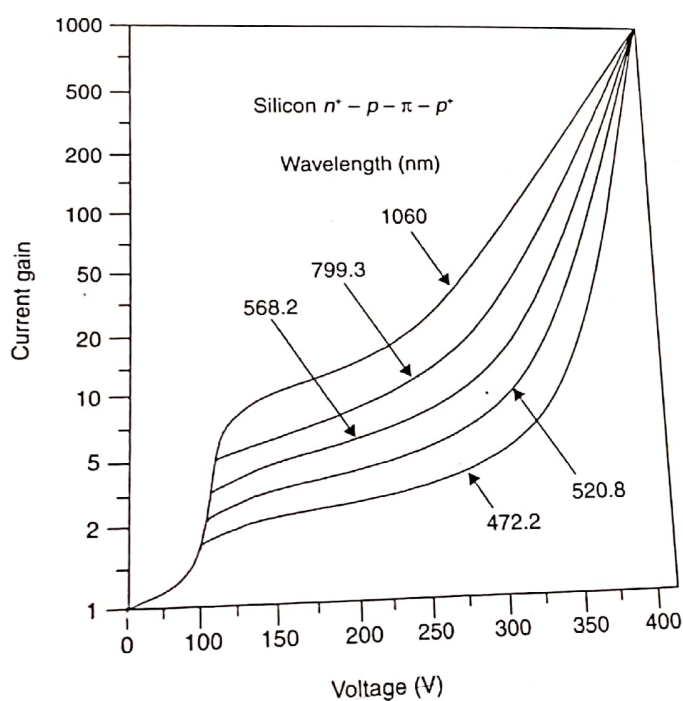


Figure 4-9. Photocurrent gain v. reverse biasing voltage for different wavelengths.

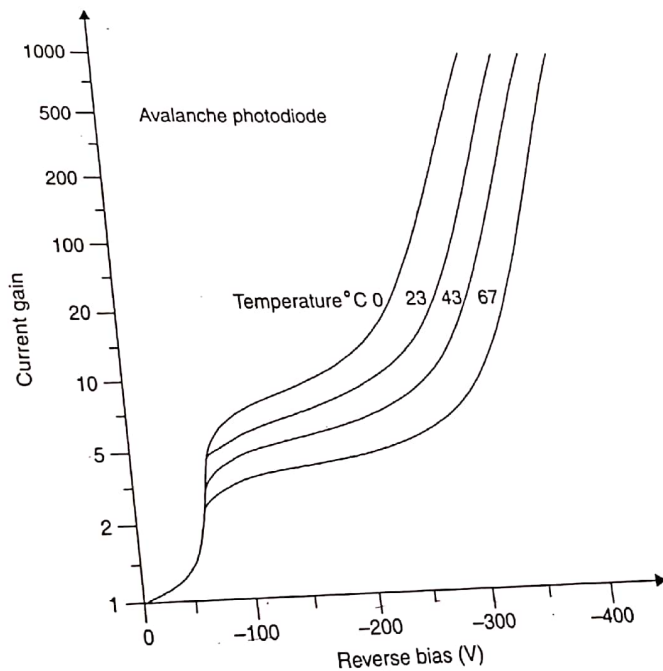


Figure 4-10. Photocurrent gain v. reverse biasing voltage at different operating temperatures.

temperature, and α is the factor determined from gain vs temperature graphs.

Photodetector Noise

Avalanche photodetectors exhibit higher noise levels than PIN devices. This is a result of the ionization and photocurrent multiplication process that takes place within the APD device. The random nature of the incident photons on the APD device results in a random photocurrent generation at the output of the device. This current fluctuation is classified as shot noise, and can be expressed in Equation (4-22).

$$\frac{d(i_p)^2}{df} = 2qI(M)^2 \quad (4-22)$$

where $(i_p)^2$ = mean square spectral density, f = frequency (Hz), q = electron charge (1.6×10^{-19} C), I = primary photocurrent, $(M)^2$ = mean square avalanche gain. The primary photocurrent can be found through the relationship $I = i_p + I_{BR} + I_{dk}$, where i_p is the photocurrent, I_{BR} is the background current, and I_{dk} is the dark current.

Equation (4-22) can be further modified to incorporate the gain nonlinearities resulting from the statistical nature of the ionization and avalanche processes (Equation (4-23)).

$$\frac{d(j_p)^2}{df} = 2qI(M)^2F(M) \quad (4-23)$$

where M is the multiplication factor, $F(M)$ is the excess noise factor, I is the primary photocurrent, (j_p) is the mean square spectral density, and f is the frequency. The excess noise factor ($F(M)$) is related to the semiconductor material used in the fabrication of the APD device, the electron-to-hole carrier ratio, and the electric field profile across the depletion region. An empirical equation determining the excess noise factor $F(M)$ is given by Equation (4-24).

$$F(M) = 2(1 - K) + K(M) \quad (4-24)$$

where M is the multiplication factor and K is the ratio of the smallest to the largest ionization coefficients

For silicon: $K \approx 0.02-0.1$

For germanium: $K \approx 0.5$

For $InGaAsP$: $K \approx 0.3-1$

Dark Current

Dark current is referred to as the current present at the photodetector output at the absence of incident light. For an APD device, the dark current is multiplied by the device multiplication factor (M) to determine the reduction in device sensitivity.

The dark current is a nonlinear function of the reverse biased voltage at avalanche breakdown levels, and is sometimes referred to as **tunneling current**. Different semiconductor materials exhibit different levels of tunneling current resulting from different band gap sizes. For example, devices with small band gaps measure small tunneling currents,

while large band gap devices measure larger tunneling currents. A practical solution for a substantial reduction of the tunneling current is the fabrication of structures with a separation between the absorption (low band gap) region and the avalanche (high band gap) region.

Response Time

The response time of a photodetector device is the time a carrier takes to cross the depletion region. For APD devices, the response time is almost double that of PIN devices. Because the APD structure incorporates a large band gap region produced by the large electric field, the generated photocarriers must travel twice the distance from the low band gap region to the higher band gap region and back, after the multiplication process has taken place. It is, therefore, evident that response time is directly related to depletion area width. The larger the width, the larger the response time. If a reduction of the depletion region is attempted in order to reduce response time, inevitably a substantial quantum efficiency reduction will result. Therefore, in APD photodetector devices, a trade-off is necessary between quantum efficiency and response time. A typical response time of 0.5 ns at 800 nm–900 nm has been achieved.

Capacitance

In a photodetector device, internal capacitance is a parasitic component that affects the overall response time of the detector. As with any other capacitance, junction capacitance of an APD device is determined by the cross-sectional area and width of its depletion region. It is expressed by Equation (4-25).

$$C = \frac{\epsilon qAN}{2(V_R + V_j)} \quad (4-25)$$

where C is the junction capacitance (F), ϵ is the dielectric constant, A is the depletion area, N is the doping density (depletion region), V_R is the reverse bias voltage (V), V_j is the junction voltage, and q is the electron charge.

4.4 PHOTODETECTOR DEVICE CHARACTERISTICS

Conventional PIN Photodetectors

Some characteristics of commercially available PIN photodetector devices are as follows:

Device type: 35PD300-FC (InGaAs photodetector)

Manufacturer: Telcom Devices

Brief description: The 35DP300-FC is an InGaAs photodetector that was designed to operate at a wavelength of 1300 nm, applicable to medium data rate optical communications systems and high sensitivity instrumentation. This device is packaged in a TO-46 header. Some of the basic device characteristics are listed in Table 4-2.

CHAPTER 4

$$R_F = (1.1 \times 10^{-3})(12.36)(1)(0.5) \times \frac{\text{failure}}{1 \times 10^6} \\ = 6.8 \times 10^{-9}$$

Therefore, $R_F = 6.8 \times 10^{-9}$.

iii) Compute MTBF.

$$\text{MTBF} = \frac{1}{R_F} = \frac{1}{6.8 \times 10^{-9}} = 147 \times 10^6$$

Therefore, MTBF = 147×10^6 hours.

4.5 ADVANCED OPTICAL SEMICONDUCTOR DEVICES

High demand optical networks require high performance optical devices. One way to improve the performance of such solid state devices is through the **resonant cavity enhancement (RCE)** method developed by (Fabry and Perot).

The utilization of the resonant microcavity principle for the design and fabrication of optical devices enhances the wavelength selectivity and resonant optical field, ultimately leading to improved quantum efficiency at the operating resonant wavelength. Furthermore, an enhanced optical field allows for a reduction of the physical dimensions of the optical device active region, and consequently increases the operating speed. Substantial improvement of operating characteristics such as high speed and wavelength selectivity qualifies optical

devices for system implementation that employs Wavelength Division Multiplexing (WDM) schemes.

RCE Detector Quantum Efficiency

Photodetector efficiency (η), or quantum efficiency, is defined as the ratio of the generated current flux to the incident photon flux, or the ratio of the power absorbed to the incident power. The increase of quantum efficiency for RCE photodetectors can be interpreted with the assistance of Figure 4-11.

An RCE device is structured with a selection of insulator and semiconductor materials such as AlAs/GaAs and InAlAs/InGaAs combined in such a way as to generate the required index differences. The absorption layer (active layer), with an absorption coefficient (α) and thickness (d), is sandwiched between two mirrors that are separated by distances L_1 and L_2 . The field reflection coefficients for both reflective mirrors are denoted as $\sqrt{R_1} e^{-j\theta_1}$ and $\sqrt{R_2} e^{-j\theta_2}$, where θ_1 and θ_2 are the phase shifts of the light penetrating the reflective mirrors.

The electric field component of the incident light wave traveling forward is composed of both the transmitted and the feedback fields. The feedback component is the result of the cavity mirror internal reflections. The wave propagation constant is given by Equation (4-31).

$$\beta = \frac{2\pi n}{\lambda_o} \quad (4-31)$$

where β is the propagation constant, n is the refractive index, and λ_o is the wavelength in vacuum. It is evident from

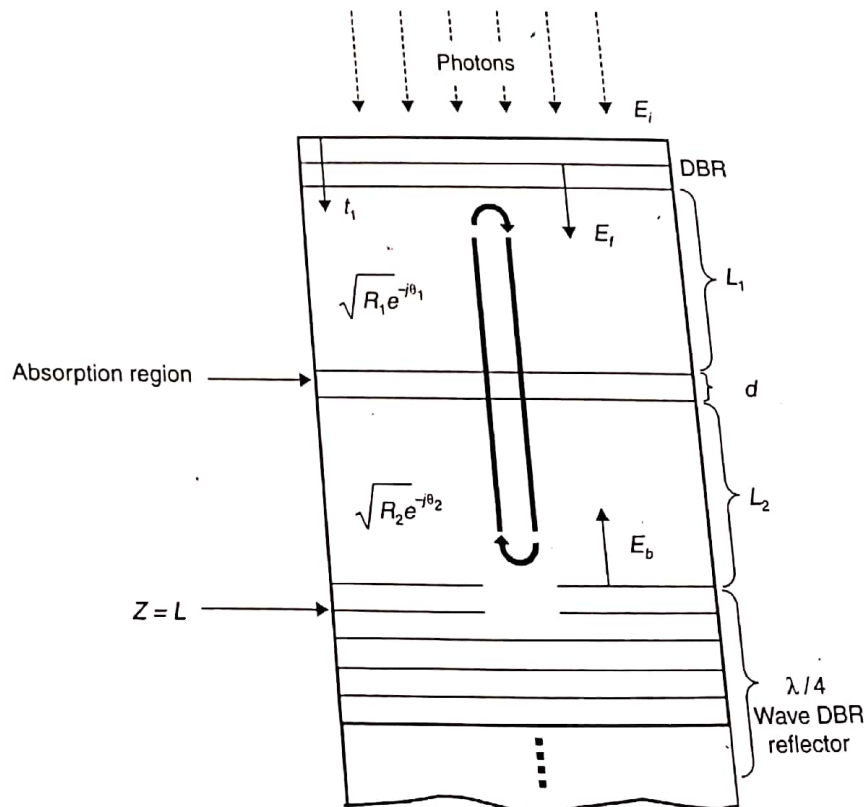


Figure 4-11. Optical detector semiconductor structure.

Quantum efficiency, is defined
to the incident photon
flux to the photodetectors

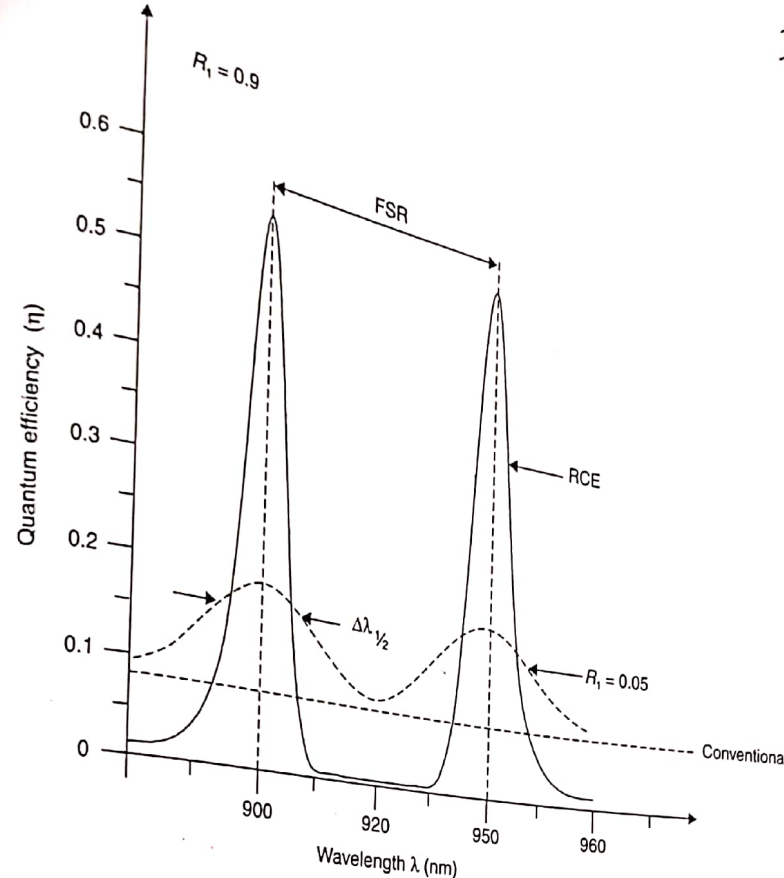


Figure 4-12. Quantum efficiency comparison between conventional optical detectors.

Equation (4-31) that the propagation constant (β) is wavelength dependent, and the refractive index (n) is periodic to the inverse wavelength (λ_o). Figure 4-12 compares the quantum efficiency (η) of both conventional and RCE photodetector devices. Photodetectors with very-close-to-unity quantum efficiency are required for specialized applications such as astronomical measurements. High quantum efficiency in photodetectors can be accomplished by a combination of high reflectivity of the bottom mirror and an absorption layer of moderate thickness. **High mirror reflection coefficients for RCE structures are very difficult to achieve.**

For conventional devices, an absorption coefficient of only a few percent can be obtained across the entire operating wavelength. For RCE devices, selecting the appropriate device parameters for the required design specifications can increase the absorption coefficient.

Compounds such as GaAs, used as bottom mirrors, exhibit a nonimpressive ninety-four percent reflectivity at approximately 1000 nm wavelength in vacuum, while metals such as Au exhibit a ninety-eight percent reflectivity under the same conditions. A combination of metal film and $1/4$ wavelength substances such as AlAs/GaAs can achieve an almost unity reflective coefficient at a desired wavelength.

The high quantum efficiency of an RCE detector device is mainly due to a substantial increase of the electric field intensity within the resonance cavity (high-Q), resulting in a higher energy absorption in the active region. This increased electric field intensity translates into a corresponding increase in much needed optical power.

The power enhancement factor of an RCE photodetector diode is shown in Figure 4-13.

Figure 4-13 shows that the power enhancement factor varies in accordance with mirror reflectivity and cavity absorption coefficients. For low cavity loss and a combination of mirror reflectivity the enhancement factor can exceed fifty percent, while for high cavity absorption and low mirror reflectivity the enhancement factor is substantially smaller.

In high Q cavities, the dramatic decrease of the enhancement factor is attributed to the higher absorption coefficient within the cavity. The thicker active layer absorbs most of the optical power. The optical power that remains is insufficient to reach the bottom mirror and is thus unable to trigger the required feedback mechanism for the enhancement process to take place.

Figure 4-14 illustrates the quantum efficiency in reference to the absorption coefficient for various levels of mirror reflectivity.

For conventional photodetector diodes with the bottom mirror reflective coefficient equal to zero, the quantum efficiency in relation to the absorption coefficient is the top line in Figure 4-14, while the RCE with the bottom mirror reflective coefficient of 0.99 is the bottom line. It is evident that the quantum efficiency of a selected wavelength is better for the RCE device than for conventional photodetector devices.

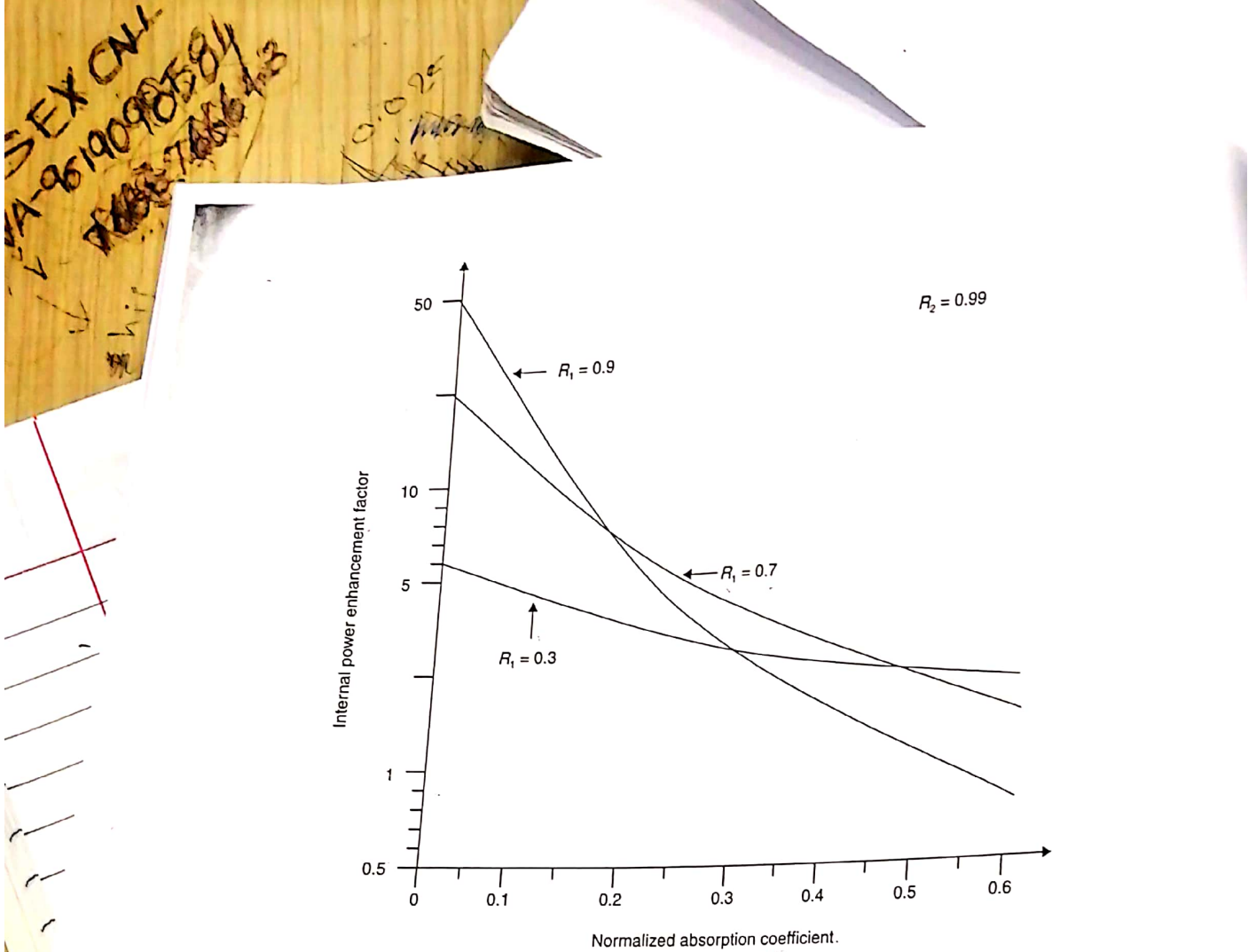


Figure 4-13. Enhanced factors for RCE photodetector diodes with $R_2 = 0.99$ and various R_1 mirror reflections.

→RCE Photodetector Wavelength Selectivity

In an RCE photodetector structure, the quantum efficiency is dramatically reduced at wavelengths outside the resonant wavelength. This is due to the mutual cancellations of both the forward and the reverse traveling waves within the resonant cavity. The spectrum between resonant peaks, referred to as the **free spectral range**, is expressed by Equation (4-32).

$$f_{sr} = \frac{\lambda^2}{2(L + L_{eff_1} + L_{eff_2})n_{eff}} \quad (4-32)$$

where f_{sr} is the **free spectral range**, λ is the wavelength, L_{eff_1}, L_{eff_2} is the **mirror effective lengths**, n_{eff} is the mirror refractive index, and L is the **active layer length**. The mirror reflective length is wavelength dependent. The length of a quarter wave mirror stack composed of GaAs/AlGaAs is around 700 nm.

Wavelength selectivity of an RCE photodetector device can be measured as the free spectral-to- $\Delta\lambda_{1/2}$ ratio, and is given by Equation (4-33).

$$\frac{f_{sr}}{\Delta\lambda_{1/2}} = \frac{\pi(R_1 R_2)^{1/4} e^{-ad}}{1 - \sqrt{R_1 R_2} e^{-ad}} \quad (4-33)$$

where R_1, R_2 is the mirror refractive index and ad are **absorption coefficients**. From Equation (4-33), it is evident that

RCE photodetector wavelength selectivity greatly depends on high mirror reflectivity and thin layers of active (absorption) region.

With typical mirror reflectivity indexes of 0.985 for the top mirror, and 0.99 for the bottom mirror, and an absorption coefficient of one percent, the ratio of f_{sr} to $\Delta\lambda_{1/2}$ can be as high as one hundred (high wavelength selectivity).

Figure 4-15 illustrates the wavelength dependency of the mirror length for a GaAl/AlGaAs mirror stack.

→Material Requirements for RCE Photodetectors

From the brief description of RCE photodetectors, it is evident that their performance depends strongly on minimum cavity loss.

For minimum cavity loss, cavity materials must be selected from those that exhibit zero absorption coefficients. Both reflective mirrors must also exhibit zero absorption coefficients as well as high mirror reflectivity. Another critical element in the design and fabrication of RCE photodetectors is the mirror thickness. The thickness of a stack of mirrors, of a total width of $\lambda/4$, must not exceed a few micrometers.

The lattice structure of cavity materials must be absolutely perfect in order to have a defect-free active layer. Furthermore, the fabrication complexity of RCE devices can

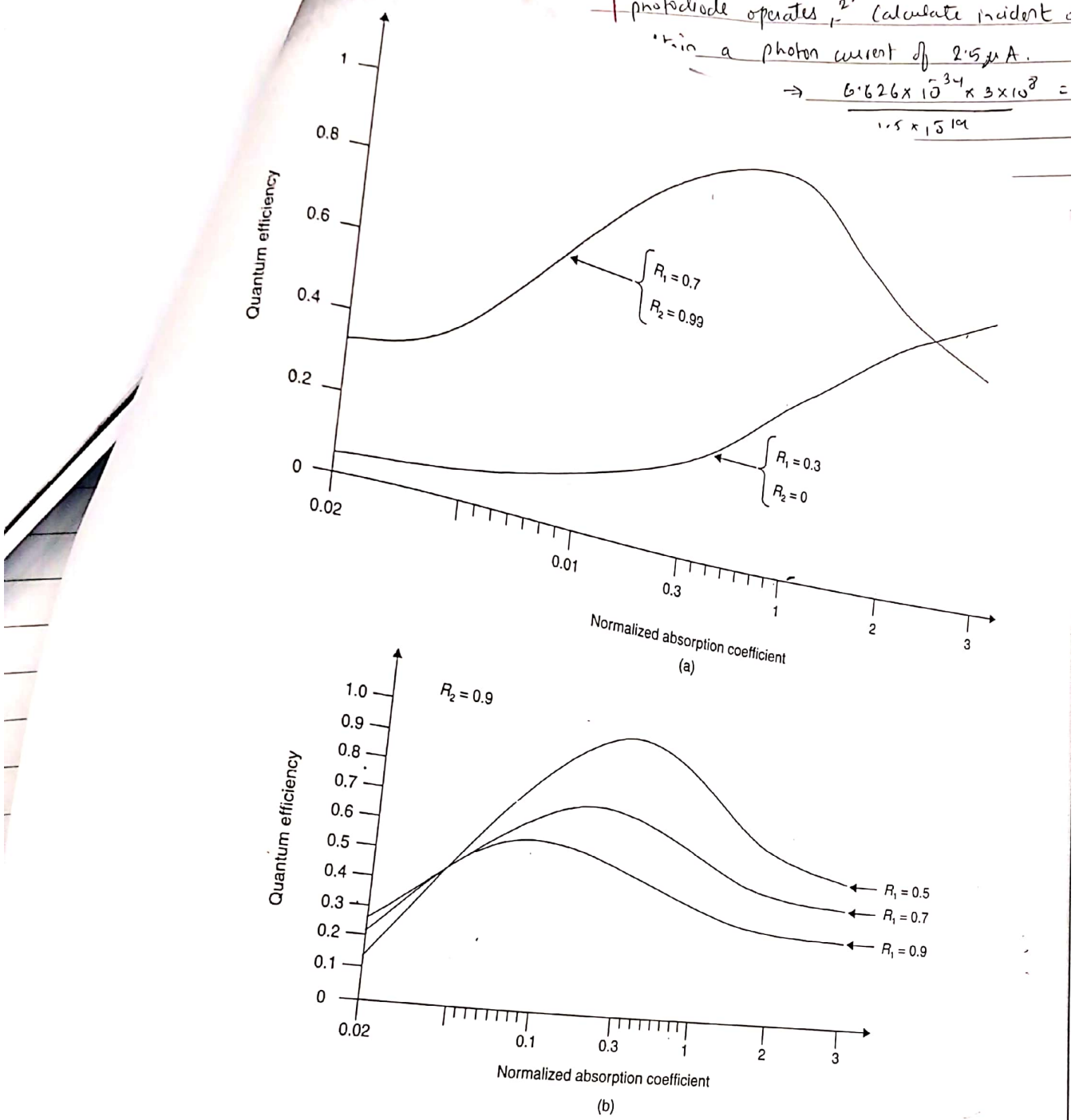


Figure 4-14. (a) Quantum efficiency v. absorption coefficient for a conventional device ($R_1 = 0.3, R_2 = 0$) and an RCE device ($R_1 = 0.7, R_2 = 0.99$). (b) Quantum efficiency v. absorption coefficient for different levels of mirror reflectivity.

be somewhat simplified if the number of mirror periods is kept to an absolute minimum. This can be accomplished by selecting a large refractive index difference among the materials that compose the reflecting mirrors.

Both cavity and mirror materials must have a larger band gap than the active region. There is, however, a low band gap limit for the active layer beyond which extraction of the photo-generated carriers will be inhibited by the heterojunction band effects. The absorption coefficient of the active layer must be between $1 \times 10^3 \text{ cm}^{-1}$ and $5 \times 10^4 \text{ cm}^{-1}$ across the operating wavelength. For larger absorption coef-

ficients, a very thin active layer is required. The negative effects of such a thin active layer are undesired electric field standing waves and a substantial reduction in the breakdown voltage. Thicker active layers reflect higher transit times and, consequently, lower device speeds.)

For RCE photodetector diodes, to achieve low noise for high speed applications, low surface recombination and high current saturation velocities must be considered. High carrier velocities can reduce transit time delays. High carrier velocities are the result of higher biasing voltages. Low recombination rates result in corresponding reduction of the

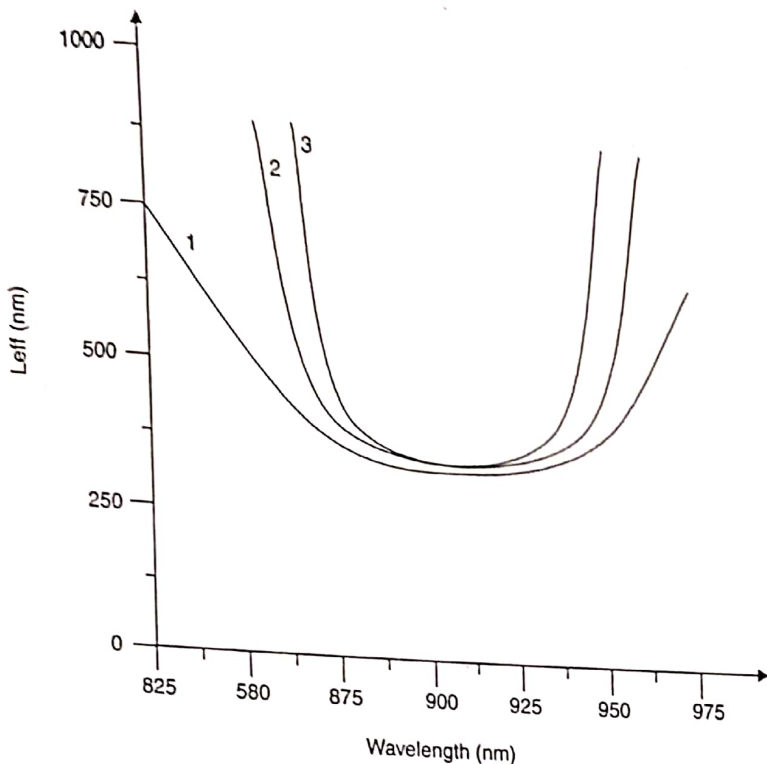


Figure 4-15. Wavelength dependency of a GaAl/GaAs stack.

dark current and detector noise. On the other hand, in order to achieve high operating bandwidths, the surface area of the device must be reduced. Surface reduction increases surface recombination and, consequently, higher dark current and detector noise. Therefore, it is imperative that a balance be maintained between surface area of the device, dark current, and detector noise and operating bandwidth.

All the criteria outlined above for the successful design and fabrication of RCE photodetector diodes can be satisfied by the combination of different semiconductor materials that operate at wavelengths of 1550 nm and beyond. A short list of such combined materials and their properties are shown in Table 4-10.

→ High Speed Comparison of Conventional and RCE Photodetectors

Speed limitations for heterojunction PIN photodetector devices are caused by several factors such as charging and discharging time of parasitic and inherent capacitances, charge trapping at the heterojunction, and **transit time** across the depletion region.

Improved fabrication techniques have successfully reduced the impacts of charge trapping at the heterojunction and diffusion time. The most serious problem—transit time and parasitic capacitance charging and discharging time—must, therefore, be used to compare the high speed performances of conventional and RCE photodetectors.

HIGH SPEED PERFORMANCE OF CONVENTIONAL DEVICES. For a conventional photodetector device (thin active layer), transit time is given by Equation (4-34).

$$t_r = 0.45 \frac{v_e}{W} \quad (4-34)$$

where t_r is the transit time(s), v_e is the electron velocity (m/s), and W is the width of the depletion region (m). When a GaAs substance with a hole velocity (v_e) of 6×10^6 cm/s is the active layer, it will require a depletion width (W) of 0.6 μm . It is evident that a decrease in the thickness of the active layer will increase the parasitic capacitance and, consequently, limit the device operating bandwidth.

The operating bandwidth of a conventional photodetector device, based on its physical characteristics (surface area) and parasitic capacitance, is given by Equation (4-35).

$$B_w = \frac{CW}{2\pi\epsilon_r\epsilon_0 R_t A} \quad (4-35)$$

where W is the depletion width, ϵ_r is the relative permittivity, ϵ_0 is the permitivity of free space, R_t is the total load and conduct resistance, A is the surface area of the device, and C is the parasitic capacitance. It is evident from Equations (4-34) and (4-35) that, for each combination of device surface area (A) and total resistivity (R), there can be an optimum depletion layer width (W) at a predetermined operating bandwidth (B_w).

Figure 4-16 shows the peak operating bandwidth of two conventional photodetector devices with dimensions $5 \mu\text{m} \times 5 \mu\text{m}$ and $10 \mu\text{m} \times 10 \mu\text{m}$ and with different surface areas and different depletion layer thicknesses.

Figure 4-16 shows that by maintaining constant total resistivity of 50Ω for both devices, the smaller detector, which has a depletion layer thickness of 150 nm, achieves

TABLE 4-10 Properties of Selected Semiconductor Materials

| Combined Materials | Properties |
|--------------------|---|
| AlGaAs/GaAs/InGeAl | <ol style="list-style-type: none"> 1. Good electronic properties 2. Low current recombination rates 3. Excellent lattice matching to AlAs 4. Good refractive index |
| AlGaAs | Easily incorporated as a wide band gap conduct layer |
| AlAs | Good refractive index allows for mirror of almost unity reflectivity (with a twenty period wave) |
| InGaAs | <ol style="list-style-type: none"> 1. Active layer material 2. With GaAs/AlAs mirrors, can extend spectral wavelength to 1550 nm 3. Active layer thickness detrimental to detector performance 4. Important for testing and prototypes 5. Limited commercial application |
| InP/InGaAs/InAlAs | <ol style="list-style-type: none"> 1. The InGaAs alloy (lattice) matches the InP substrate perfectly 2. Exhibits excellent electrical properties 3. Covers the wavelength spectrum between 1300 nm and 1550 nm 4. Exhibits a poor refractive index between InAlAs and InGaAs 5. To achieve near unity mirror reflectivity, approximately 35 periods are required 6. InP/InGaAlAs very promising alloys for future commercial applications |
| AlAs/GaAs/Ge | <ol style="list-style-type: none"> 1. The use of Ge as an active layer extends the operating wavelength beyond the 1550 nm range 2. Ge exhibits moderate absorption coefficients beyond the 1000 nm range 3. Ge exhibits very low recombination rates 4. Very difficult to grow GaAs on Ge |
| Si/SiGe | <ol style="list-style-type: none"> 1. Si RCE photodetectors are commonly used at wavelengths below 1000 nm 2. Si as active layer, in conjunction with SiGe alloys, is used for longer wavelengths 3. Quarter mirrors exhibit good potentials at wavelengths below 1000 nm 4. Moderate absorption rates at 1000 nm 5. Operate with optimum performance at 1500 nm |
| Si/AlP/GaP | <ol style="list-style-type: none"> 1. Operate successfully over the visible wavelength span 2. On the negative side, the refraction index between AlP and GaP is somewhat smaller than that of GaAs/AlAs. Increasing the number of mirror periods and using thinner mirrors for shorter wavelength applications can compensate for the negative effect |

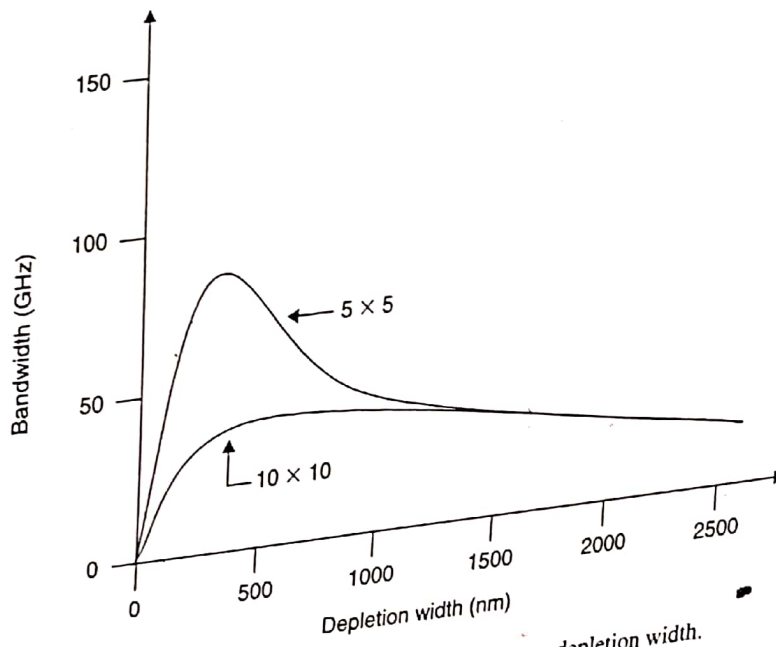


Figure 4-16. Conventional photodetector diode operating bandwidth dependency on depletion width.

CHAPTER 4

a peak bandwidth of 86 GHz. The larger device, which has a depletion layer thickness of 300 nm achieves a peak bandwidth at 43 GHz. The peak bandwidth is directly proportional to the depletion layer thickness.

HIGH SPEED PERFORMANCE OF RCE PHOTODETECTORS. The improvement factor of the limiting bandwidth performance of RCE photodetector devices is attributed mainly to innovative design and improved fabrication techniques.

In such a PIN semiconductor structure, a small band gap absorption layer with thickness (D) is placed in the depletion region (Figure 4-17).

Figure 4-17 shows that the carriers (electrons and holes) must travel a smaller distance in an RCE than in a conventional structure. The transit time for both carriers is expressed by Equations (4-36a) and (4-36b).

$$t_e = \frac{W_1}{v_e} \quad (4-36a)$$

$$t_h = \frac{W_2}{v_h} \quad (4-36b)$$

where W_1 is the distance traveled by the electrons, W_2 is the distance traveled by the holes, v_e is the velocity of the electron, and v_h is the velocity of the hole. The limited bandwidth (B_w) for an RCE photodetector is given by Equation (4-37).

$$B_w = 0.45 \frac{v_e + v_h}{W + D} \quad (4-37)$$

when $D < W$ and $v_e > v_h$ in a GaAs substance, electron velocity (v_e) is 1×10^7 cm/s.

Comparing Equations (4-36) and (4-37), it is evident that the limited operating bandwidth of an RCE photodetector is significantly higher than the limited bandwidth of a conventional device.

where L_d is the decay, and ad are absorption co-eff.

Example 4-3

Compute the photon lifetime inside an RCE P diode with the following characteristics.
 $R_1 = 0.7$
 $R_2 = 0.99$
 $ad = 0.1$

Solution
i) Compute decay'

Photon Lifetime

Another important factor contributing to RCE photodetector diode bandwidth limiting performance is the **photon lifetime** (t_{ph}). Photon lifetime is defined as the time required for the building or decaying of the optical field within the resonant cavity, and is expressed by Equation (4-38).

$$t_{ph} = \frac{t_r}{L_d} \quad (4-38)$$

where t_{ph} is the photon lifetime (s), t_r is the total photon round trip (s), and L_d is the **decay losses** during the round trip. Experimental results have shown that for a GaAs cavity with a length of 1000 nm, the total photon round trip is approximately 23 fs (23×10^{-15} s). Decay losses (L_d) are given by Equation (4-39).

$$L_d = 1 - R_1 R_2 e^{-2ad} \quad (4-39)$$

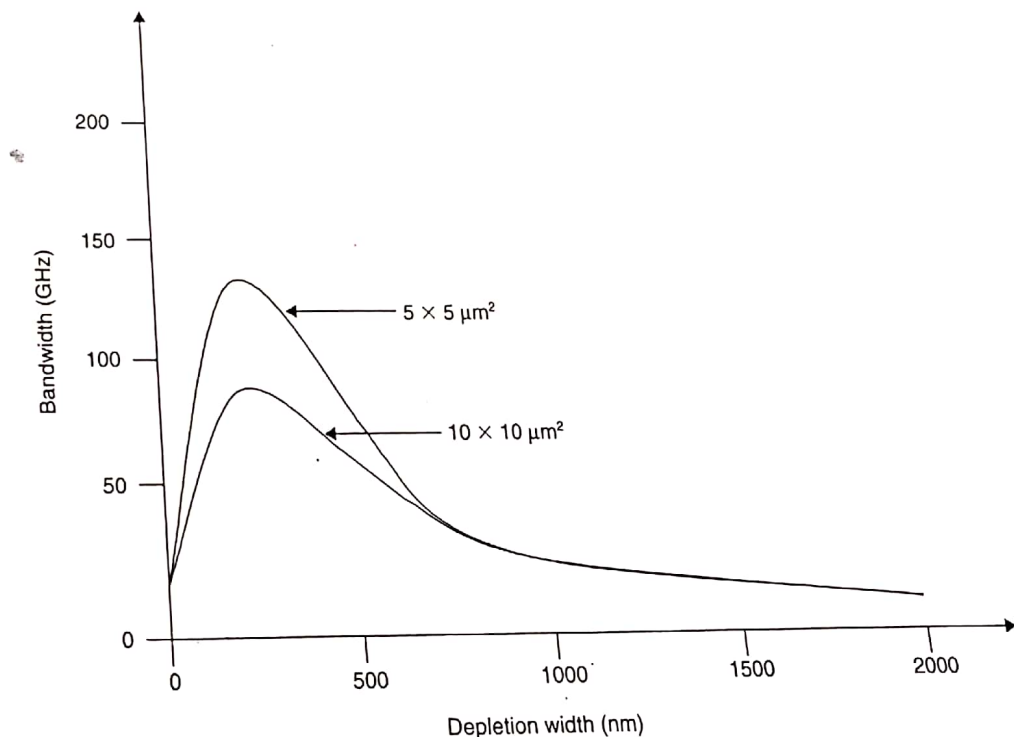


Figure 4-17. RCE photodetector diode bandwidth dependency on depletion width.

(4-37)
tron velocity
evident
ode.
of

where L_d is the decay loss, R_1, R_2 is the mirror reflectivity, and ad are absorption coefficients.

Example 4-3
Compute the photon lifetime inside an RCE photodetector diode with the following characteristics:

$$R_1 = 0.7$$

$$R_2 = 0.99$$

$$ad = 0.1$$

Solution

i) Compute decay losses (L_d).

$$\begin{aligned} L_d &= 1 - R_1 R_2 e^{-2ad} \\ &= 1 - (0.7)(0.99) e^{-2(0.1)} \\ &= 0.4326 \end{aligned}$$

Therefore, $L_d = 0.4326$.

ii) Compute photon lifetime (t_{ph}).

$$t_{ph} = \frac{t_{rt}}{L_d} = \frac{40 \text{ fs}}{0.4326} = 92.46 \text{ fs}$$

Therefore, $t_{ph} = 92.46 \text{ fs}$, assuming a total photon round trip within the cavity of 40 fs.

The RCE photodetector device bandwidth limit is based on photon lifetime decay as follows.

$$B_w = \frac{1}{t_{ph}} = \frac{1}{92.46 \times 10^{-15} \text{ s}}$$

$$B_w = 10.8 \text{ THz}$$

Therefore, $B_w = 10.8 \text{ THz}$

It is evident that the photon lifetime component is critical only at the THz range.

RCE Schottky Photodiodes

Researchers have been aware, since 1995, that placing a conventional Schottky photodetector semiconductor device (InAlAs) into a Fabry-Perot resonant cavity can greatly enhance the device performance. By employing a thinner absorption region, a significant reduction of the transit time was observed, with a parallel increase of quantum efficiency at resonant wavelength.

Laboratory experimentation has demonstrated that an RCE structure using an InP substrate to grow an InAlAs/InGaAlAs eight-period mirror, with an absorption region composed of a 475 nm InGaAs, a 50 nm AlInAs Schottky layer, and a high reflectivity Al Schottky layer for conduct, an impressive increase of detector photocurrent in comparison to standard Schottky photodiode structures results.

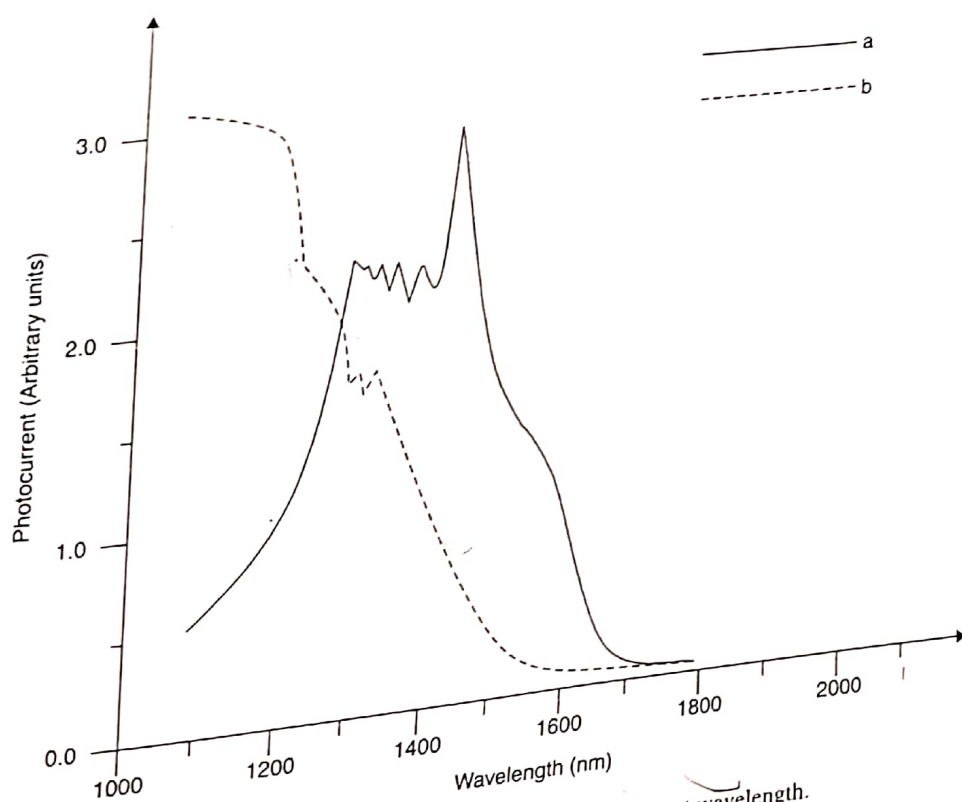


Figure 4-18. RCE and standard Schottky photodetector current performance at resonant wavelength.

Figure 4-18 shows a significant increase of RCE photodetector current at resonant wavelength in comparison to that of a standard Schottky photodetector diode.

RCE Avalanche Photodiodes

Applying the RCE concept to the design and fabrication of an APD photodetector device results in an optimum quantum efficiency bandwidth product. One of the fundamental bandwidth limiting factors of a standard APD photodetector device is the transit time of the secondary electrons that travel through the depletion region. If the transit time is somehow reduced, the overall device operating bandwidth will be substantially increased.

The other component that is crucial in determining device performance is the quantum efficiency. An increase in

quantum efficiency will enhance the photodetector quantum efficiency bandwidth product. This increase in quantum efficiency can be achieved by employing a thinner absorption region. A thinner absorption region also means that a larger electric field will be generated across the region, thus allowing for a proportional reduction of the externally applied DC biasing, and consequently, lower power supply voltage. An RCE based APD photodetector is illustrated in Figure 4-19.

Figure 4-19 illustrates an early RCE APD photodetector structure composed of a very thin (900 \AA) absorption layer that is located in the optical cavity of a fifteen quarter-wave AlAs/GaAs mirror that has an approximate reflectivity factor of ninety percent at a predetermined wavelength. The performance of this device was measured with different mirror reflectivity and the result is shown in Figure 4-20.

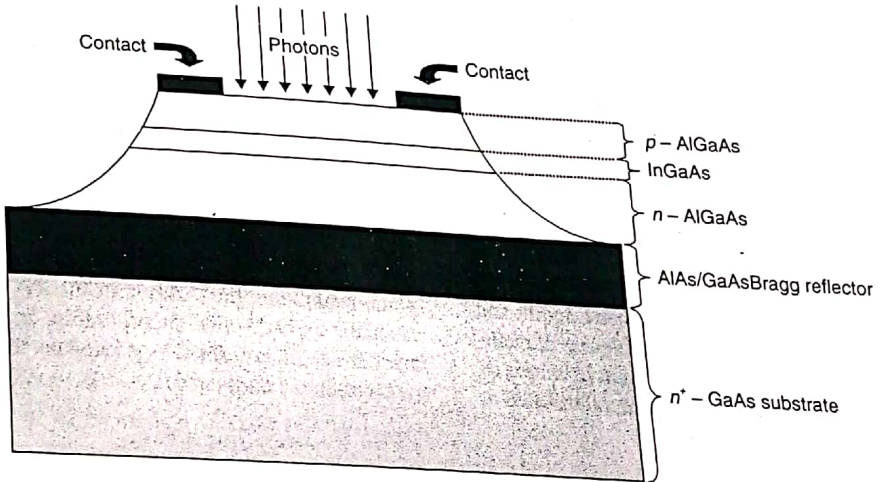


Figure 4-19. An RCE based APD photodetector structure.

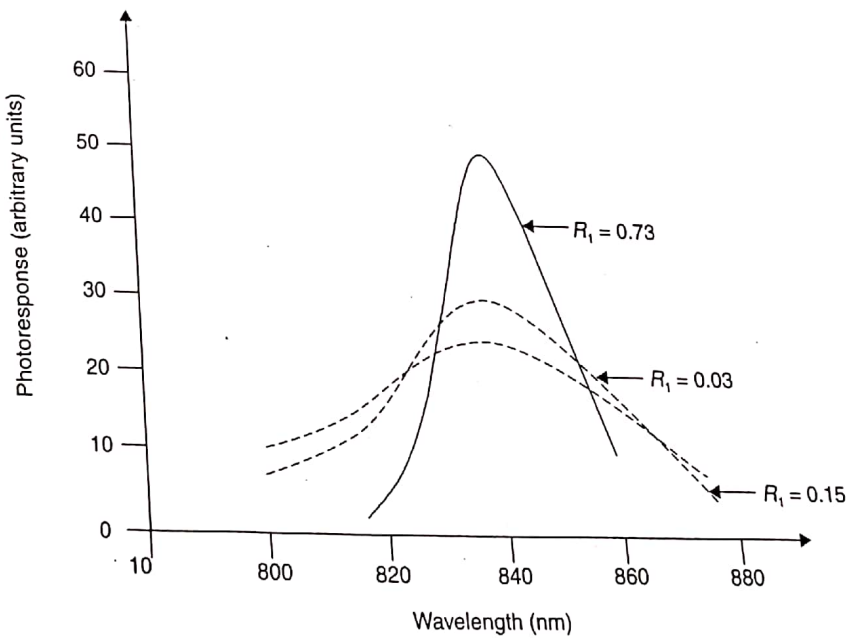


Figure 4-20. RCE APD photoresponse at different mirror reflective indexes.

Figure 4-20 illustrates that maximum quantum efficiency can be achieved at a specific high reflectivity contributes to the enhancement of quantum efficiency. Therefore, a better lower mirror reflectivity generates high gain was attributed to the thin layer itself. A gain of close to nine times was measured with a reflectivity of nine percent.

RCE P
For

Figure 4-20 illustrates that maximum quantum efficiency can be achieved at a specific high Q of the resonant cavity and at a high mirror reflective index. A bottom mirror low reflectivity contributes to the quantum efficiency limit. Therefore, a better lower mirror reflectivity can substantially enhance quantum efficiency. In the same device, photodetector gain was measured and found to be very high. This high gain was attributed to the thin absorption layer. Such a thin layer generates a comparatively high electric field across itself as a function of the external DC biasing voltage. A gain of close to two hundred was measured at a DC biasing of nine volts.

RCE PIN Photodetector Devices

For very high-speed optical detectors (above the 100 GHz range) conventional PIN devices exhibit compatible characteristics. The only disadvantage is their low sensitivity. Low sensitivity can be remedied by introducing the RCE PIN photodetector diode.

The first RCE PIN device was composed of an InGaAs/InGaAsP/InP structure with a 200 nm InGaAs absorption layer. This device exhibited a quantum efficiency of 82% at the 1550 nm operating wavelength. Mirror reflectivity was set at $R_1 = 0.95$ and $R_2 = 0.7$. The cross section of this structure is illustrated in Figure 4-21.

Various researchers experimenting with substances such as SiGe based RCE PIN structures noticed a significant reduction in quantum efficiency. The limited degree of quantum efficiency was due to the small refractive index of Si/SiGe mirrors. Further experimentation demonstrated a

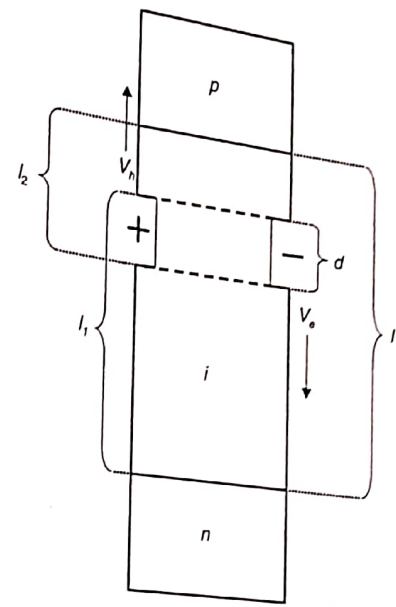


Figure 4-21. An RCE PIN photodetector diode.

significant improvement (over 30%) in quantum efficiency when optimizing the location of the absorption layer in the resonant cavity, while incorporating a thinner absorption layer in an InGaAs/InAlAs photodetector structure significantly reduced dark current.

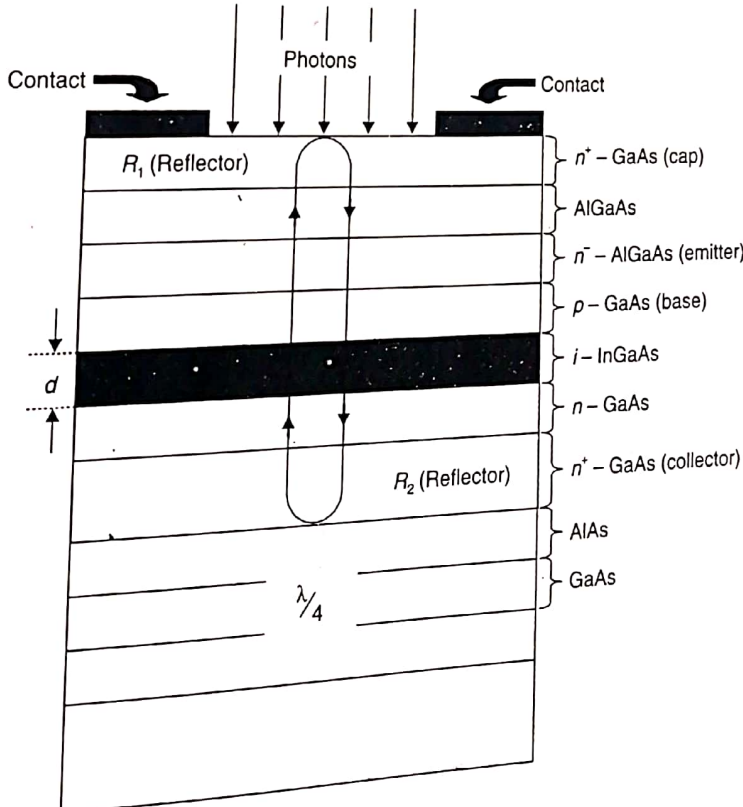


Figure 4-22. An RCE HPT detector/amplifier combination.

RCE Heterojunction Phototransistors

In high density optical fiber communications systems, amplifiers coupled to the output of optical detectors are highly desirable. Such a combination of photodetectors and optical amplifiers, exhibiting high gain and low noise as required by high density optical systems, can be accomplished through the combination of RCE structure with heterojunction transistors.

An RCE HPT detector/amplifier combination that employs AlGaAs/GaAs substances for the heterojunction and InGaAs for the active layer was tested experimentally. The cross section of such a device is illustrated in Figure 4-22.

The early and experimental optical detector/amplifier combination pictured in Figure 4-22 employed a top mirror composed of a GaAs substrate with a 30% reflectivity, a bottom mirror composed of ten AlAs/GaAs substrate stacks with a 90% reflectivity, and an active layer of 100 nm width composed of InGaAs materials.

The high gain of this device was mainly due to nonexisting cavity loss and a large photocurrent generation of 900 nm at the resonant wavelength. The relatively smaller gain shown at the 850 nm wavelength is mainly at

tributed to small cavity losses. For an improved quantum efficiency and wavelength sensitivity of the RCE HPT device, a larger Fabry-Perot cavity is required. In such a device, operating at the 930 nm wavelength, InGaAl quarter wavelengths are optimally placed in a high Q Fabry Perot cavity with mirror reflectivity of 99% and 70% for R_2 and R_1 , respectively. The device exhibited very high gain and excellent photoresponse. Heterojunction phototransistors composed of InGaAs/InAlAs/In and operating at 1300 nm and 1600 nm, with an Au high reflectivity mirror, have exhibited very high optical gain.

SUMMARY

In Chapter 4, the concept of photodetection and its application in the design of optical receivers was presented. A detailed examination of the two major types of photodetector diodes (PIN and avalanche) was performed in terms of fabrication, optical gain, noise, and response time. The chapter concluded with an introduction of advanced photodetector diodes, including the RCE and RCE HPT. In order to reinforce the concepts, numerous examples were given throughout the chapter.

QUESTIONS

Section 4.1

1. Define *photodetection process*.
2. What is the role of the optical detector in a fiber optics communications system?
3. Name the fundamental performance characteristics of optical detectors.
4. What are the basic criteria for the selection of a photodetector diode to be incorporated in the design of an optical receiver?
5. Name the two basic types of photodetector diodes.

Section 4.2

6. What does the acronym *PIN* mean?
7. Briefly describe the principal theory upon which the operation of a PIN photodiode is based.
8. Draw a schematic of a silicon PIN diode and explain its operation.
9. What are the parameters involved in the establishment of the cut off frequency of a semiconductor material employed in the fabrication of a PIN photodetector?
10. List the PIN diode's basic characteristics.
11. Define *quantum efficiency* and its relation to PIN efficiency.
12. Define *response time* of a photodiode.

13. What are the main factors that contribute to response time?
14. With the assistance of a graph, explain the relationship between wavelength, responsivity, and quantum efficiency.
15. What is *dark current*?
16. Describe *shot-noise*.
17. With the assistance of a formula, describe *noise power*.
18. What is *Johnson noise*?
19. Define *signal to noise ratio (SNR)*. Give an example.
20. Describe the negative effect of dark current in the operation of a PIN photodiode.
21. How can the performance of a PIN device be enhanced through the reduction of the level of dark current?

Section 4.3

22. What is an *avalanche photodetector*?
23. How do avalanche photodetectors differ from PIN diodes?
24. What is the *multiplication factor* and what is its dependency?
25. Draw the physical layout of an APD silicon diode and briefly explain its operation.